Tissue compartmentalization enables *Salmonella* persistence during chemotherapy

Jiagui Li[a,1], Beatrice Claudi[a,1], Joseph Fanous[a,1], Natalia Chicherova[a], Francesca Romana Cianfanelli[a], Robert A. A. Campbell[a], and Dirk Bumann[a,2]

[a]Biozentrum, University of Basel, CH-4056 Basel, Switzerland

Edited by Jorge Galán, Department of Microbial Pathogenesis, Yale University, New Haven, CT; received July 28, 2021; accepted November 11, 2021

Antimicrobial chemotherapy can fail to eradicate the pathogen, even in the absence of antimicrobial resistance. Persisting pathogens can subsequently cause relapsing diseases. In vitro studies suggest various mechanisms of antibiotic persistence, but their in vivo relevance remains unclear because of the difficulty of studying scarce pathogen survivors in complex host tissues. Here, we localized and characterized rare surviving *Salmonella* in mouse spleen using high-resolution whole-organ tomography. Chemotherapy cleared >99.5% of the *Salmonella* but was inefficient against a small *Salmonella* subset in the white pulp. Previous models could not explain these findings: drug exposure was adequate, *Salmonella* continued to replicate, and host stresses induced only limited *Salmonella* drug tolerance. Instead, antimicrobial clearance required support of *Salmonella*-killing neutrophils and monocytes, and the density of such cells was lower in the white pulp than in other spleen compartments containing higher *Salmonella* loads. Neutrophil densities declined further during treatment in response to receding *Salmonella* loads, resulting in insufficient support for *Salmonella* clearance from the white pulp and eradication failure. However, adjunctive therapies sustaining inflammatory support enabled effective clearance. These results identify uneven *Salmonella* tissue colonization and spatiotemporal inflammation dynamics as main causes of *Salmonella* persistence and establish a powerful approach to investigate scarce but impactful pathogen subsets in complex host environments.

bacterial infection | antimicrobial chemotherapy | treatment failure | 3D microscopy | salmonellosis

In difficult-to-treat bacterial infections, including tuberculosis, deep-seated *Staphylococcus aureus* infections, and invasive salmonellosis, adequate antimicrobial chemotherapy can initially clear most pathogen cells and resolve clinical symptoms. However, even extended therapy often fails to eradicate the pathogen, even in the absence of relevant antimicrobial resistance. The persistence of a small subset of pathogen cells can cause relapsing diseases and accelerates the emergence of antimicrobial resistance (1–4). Eradication of such difficult-to-treat infections represents an urgent medical need.

Development of effective treatments requires a detailed understanding of the underlying mechanisms. Various mechanisms have been proposed to explain pathogen persistence during antimicrobial chemotherapy. First, antimicrobials might not reach all bacterial cells in sufficient amounts because anatomical permeation barriers limit drug access to bacteria in certain tissue areas (5, 6). Second, bacteria might adopt physiological states in host tissues that enable them to tolerate antibiotic exposure. Such tolerant states might be triggered by stresses imposed on the pathogen by the host immune system (7–13). Moreover, limited nutrient supply and stress conditions can slow bacterial proliferation, which increases tolerance to most antibiotics (14–18), in some conditions due to low ATP levels (19). Third, pathogen heterogeneity has been suggested as a major cause of treatment failures (1, 2, 20–22). Some bacteria might stop replication either because of stochastic internal processes or in response to external triggers. Such nonreplicating "persisters" can survive exposure to otherwise lethal antibiotic concentrations. Other forms of heterogeneity might also contribute to treatment failures, including asymmetric cell division (23–25), uneven partitioning of efflux pumps among daughter cells (26), heterogeneous expression of prodrug-activating enzymes (27), transient gene amplification (28), and heterogeneous induction of specific stress responses (29). The relevance of these various mechanisms for pathogen persistence in host tissues remains unclear because supporting data have been obtained almost exclusively using in vitro models (1–3, 20–22, 30). In vivo data are critical because bacterial susceptibility depends on environmental factors, and complex and diverse microenvironments in infected tissues are difficult to mimic in vitro (31).

One suitable small-animal infection model for in vivo studies is systemic salmonellosis in mice as a model for human invasive *Salmonella* infections. Such infections, including typhoid and paratyphoid fever (enteric fever) as well as nontyphoidal *Salmonella* (NTS) bacteremia, are a major health problem worldwide (32, 33). Antimicrobial chemotherapy frequently fails to eradicate *Salmonella*, resulting in relapsing disease, even when the bacterial strain is susceptible to the drug (34–37). Mouse models of invasive salmonellosis recapitulate these eradication

Significance

Some infections are exceedingly difficult to cure, even with adequate antimicrobial chemotherapy. How pathogens can survive exposure to antimicrobials in tissues remains poorly understood. Using three-dimensional whole-organ tomography, we show that *Salmonella* colonization of the mouse spleen is uneven. Low *Salmonella* density in the white pulp triggers only limited local infiltration by inflammatory cells that are crucial for supporting antimicrobial *Salmonella* clearance. Inflammatory cell density declines further during treatment in response to receding *Salmonella* loads, resulting in insufficient support for clearance and eradication failure. However, sustaining inflammation during antimicrobial chemotherapy enables effective clearance. Our findings identify heterogeneous host–pathogen interactions in compartmentalized tissues as a main mechanism underlying the antibiotic persistence of *Salmonella*.

Author contributions: J.L., B.C., J.F., and D.B. designed research; J.L., B.C., J.F., and F.R.C. performed research; N.C., F.R.C., and R.A.A.C. contributed new reagents/analytic tools; J.L., B.C., J.F., N.C., F.R.C., and D.B. analyzed data; and J.L. and D.B. wrote the paper.

The authors declare no competing interest.

This article is a PNAS Direct Submission.

[1]J.L., B.C., and J.F. contributed equally to this work.

[2]To whom correspondence may be addressed. Email: dirk.bumann@unibas.ch.

This article contains supporting information online at http://www.pnas.org/lookup/suppl/doi:10.1073/pnas.2113951118/-/DCSupplemental.

Published December 15, 2021.

MICROBIOLOGY

challenges (38–41). We showed previously that clinically relevant doses of fluoroquinolone antibiotics clear *Salmonella* from mouse tissues only slowly because *Salmonella* replicates slowly in vivo with generation times around 6.5 h (42). Nevertheless, clearance continues with a monophasic exponential decay of colony-forming units (CFUs) for at least 5 d. Here, we continued treatment for longer intervals and observed declining clearance rates and eradication failure at later time points. We aimed at unraveling the mechanisms underlying this antibiotic persistence of *Salmonella*.

In vivo studies of pathogen cells surviving chemotherapy have been thwarted by difficulties in localizing and characterizing few, sparsely distributed, micrometer-sized pathogen cells in entire centimeter-sized host organs. We addressed these limitations by adopting serial two-photon tomography (STP) (43) for detecting individual *Salmonella* cells across entire spleens of infected mice. We resolved interfering tissue autofluorescence, developed automated pipelines for identifying *Salmonella* cells in terabytes (TB) of imaging data, and validated accurate detection of single *Salmonella* cells at densities as low as one bacterium in 100 mm^3 tissue. We used STP to localize *Salmonella* surviving treatment with two clinically relevant antibiotic classes. We combined STP with laser-capture microdissection, flow cytometry, *Salmonella* reporter constructs, and adjunctive therapies, to determine the relevance of nonreplicating *Salmonella* persisters, stress-triggered drug tolerance, uneven drug delivery, and tissue infiltration by neutrophils and inflammatory monocytes. We found that *Salmonella* colonization of spleen in untreated mice was inhomogeneous. A minor *Salmonella* subset colonized the white pulp (WP) and triggered only limited local infiltration of inflammatory monocytes and neutrophils. These *Salmonella*-killing host cells supported *Salmonella* clearance during chemotherapy, but their density collapsed during chemotherapy in response to receding local *Salmonella* loads resulting in 70-fold better *Salmonella* survival in the WP compared to other, initially more colonized and inflamed spleen compartments. By contrast, *Salmonella* dormancy, stress-induced antimicrobial tolerance, or inefficient antibiotic delivery had all minor relevance. Thus, host tissue architecture and the topology and dynamics of host–*Salmonella* interactions caused locally divergent antimicrobial activities that ultimately resulted in eradication failure.

Results

Chemotherapy Fails to Eradicate Invasive Salmonellosis. We infected genetically susceptible BALB/c mice by oral administration of *Salmonella enterica* serovar Typhimurium. Once clinical symptoms emerged, we started chemotherapy with recommended doses of the fluoroquinolone antibiotic enrofloxacin. This treatment prevented mouse mortality, resolved clinical symptoms, and diminished *Salmonella* loads in the major target-organ spleen ~200-fold with slow, monophasic exponential kinetics over 6 d (42) (Fig. 1 *A* and *B*). However, clearance decelerated thereafter, even though *Salmonella* survivor cells retained in vitro susceptibility (minimal inhibitory concentration, MIC, 0.03 to 0.06 mg per liter). After 10 d of treatment, *Salmonella* survived in the spleen (~2,000 CFUs), the liver (~2,000), the mesenteric lymph nodes (~1,000), and the Peyer's patches (~200 in the last small-intestinal patch) (SI Appendix, Fig. S1*A*). Reservoirs of surviving *Salmonella* in these and other organs have been previously observed after treatment of intravenously infected mice (38) and in a streptomycin-pretreated enteritis model with high initial *Salmonella* loads in the cecum (44).

The *Salmonella* survivors caused disease relapse upon treatment discontinuation in seven out of eight tested mice (Fig. 1 *A* and *B* and *SI Appendix*, Fig. S1*B*). A second regimen of enrofloxacin again reduced clinical symptoms to baseline (*SI Appendix*, Fig. S1*B*) indicating that *Salmonella* remained susceptible to treatment in vivo. At the end of the second regimen, we still found surviving *Salmonella* in the spleen, the liver, and the mesenteric lymph nodes but not in the last Peyer's patch (*SI Appendix*, Fig. S1*A*). Administration of enrofloxacin at doses 60- to 120-fold higher than recommended (to avoid adverse effects), still requires 5 wk for *Salmonella* eradication (39, 45, 46).

Similarly, after 10 d of treatment with the beta-lactam ceftriaxone, 480 ± 190 *Salmonella* cells survived in the spleen (*SI Appendix*, Fig. S1*C*). Relapsing disease upon treatment discontinuation occurred in all four tested mice and could be treated with a second regimen of ceftriaxone (*SI Appendix*, Fig. S1*B*). Thus, two major classes of antibiotics that are widely used to treat human invasive salmonellosis, failed to eradicate *Salmonella* in orally infected mice.

Serial Two-Photon Tomography Detects Sparse *Salmonella* in the Spleen. Our goal was to identify survival mechanisms and host microenvironments of the persisting *Salmonella*. Currently available methods (47–51) are impractical for characterizing scattered micrometer-sized *Salmonella* cells in centimeter-sized host organs. However, STP tomography provides a robust method for a similar task—the detection of thin neuronal axons with submicron resolution in entire mouse brain (43) (Fig. 1*C*). We were thus interested to adapt STP for infectious diseases. Our initial attempts showed that standard STP protocols were hampered by substantial tissue autofluorescence in the spleen that became particularly strong during infection (*SI Appendix*, Fig. S2*A*) and masked the fluorescence signal of GFP-expressing *Salmonella*. We were unable to boost GFP levels because this would diminish *Salmonella* in vivo fitness (52), but we discovered that storage of perfusion-fixed spleen in freeze protectant at −20 °C effectively suppressed the interfering tissue autofluorescence (*SI Appendix*, Fig. S2*A*). As another challenge, illumination was uneven and varied between samples (*SI Appendix*, Fig. S2*B*), precluding subtraction of a single reference background image as can be done for brain datasets. Applying "corrected intensity distributions using regularized energy minimization" (CIDRE) (53) resolved this issue (*SI Appendix*, Fig. S2*B*).

Imaging 5-mm slices of spleen at 0.435-μm horizontal and 10-μm vertical resolution (Fig. 1*D*) revealed *Salmonella*-like particles with spectral characteristics of GFP (Fig. 1*E*). A single three-dimensional (3D) image stack for a 5-mm slice of spleen contained ~0.5 TB of data, prohibiting manual analysis. Simple threshold-based *Salmonella* detection was hampered by residual autofluorescence and imaging artifacts. To resolve this issue, we utilized machine learning, including support vector machines and a deep convolutional neural network that discriminated GFP-*Salmonella* from background with >99% sensitivity and specificity. We validated the identification of GFP-*Salmonella* by antibody staining of *Salmonella* lipopolysaccharide in spleen sections retrieved from the tomograph (Fig. 1*E*) and detected no signals classified as GFP-*Salmonella* in the spleen of mice infected with yellow fluorescent protein (YFP)-*Salmonella* indicating specific detection. Collagen second-harmonic signals (54) and in vivo staining of host cell surface antigens with fluorescence-labeled antibodies revealed the tissue context of *Salmonella* cells (Fig. 1 *D* and *E*). We focused on infected spleen in this study but STP also identified GFP-*Salmonella* in liver, mesenteric lymph nodes, and small intestinal Peyer's patches (*SI Appendix*, Fig. S3 and Movies S1–S3).

Single *Salmonella* cells had a narrow GFP fluorescence-intensity distribution consistent with flow cytometry data for the same GFP-*Salmonella* strain in the spleen (55) (Fig. 1*F*), indicating reliable fluorescence quantification by STP. For unresolved *Salmonella* microcolonies, we divided total fluorescence by the median single-cell GFP value to estimate the number of *Salmonella* cells per microcolony (Fig. 1*G*). The results showed

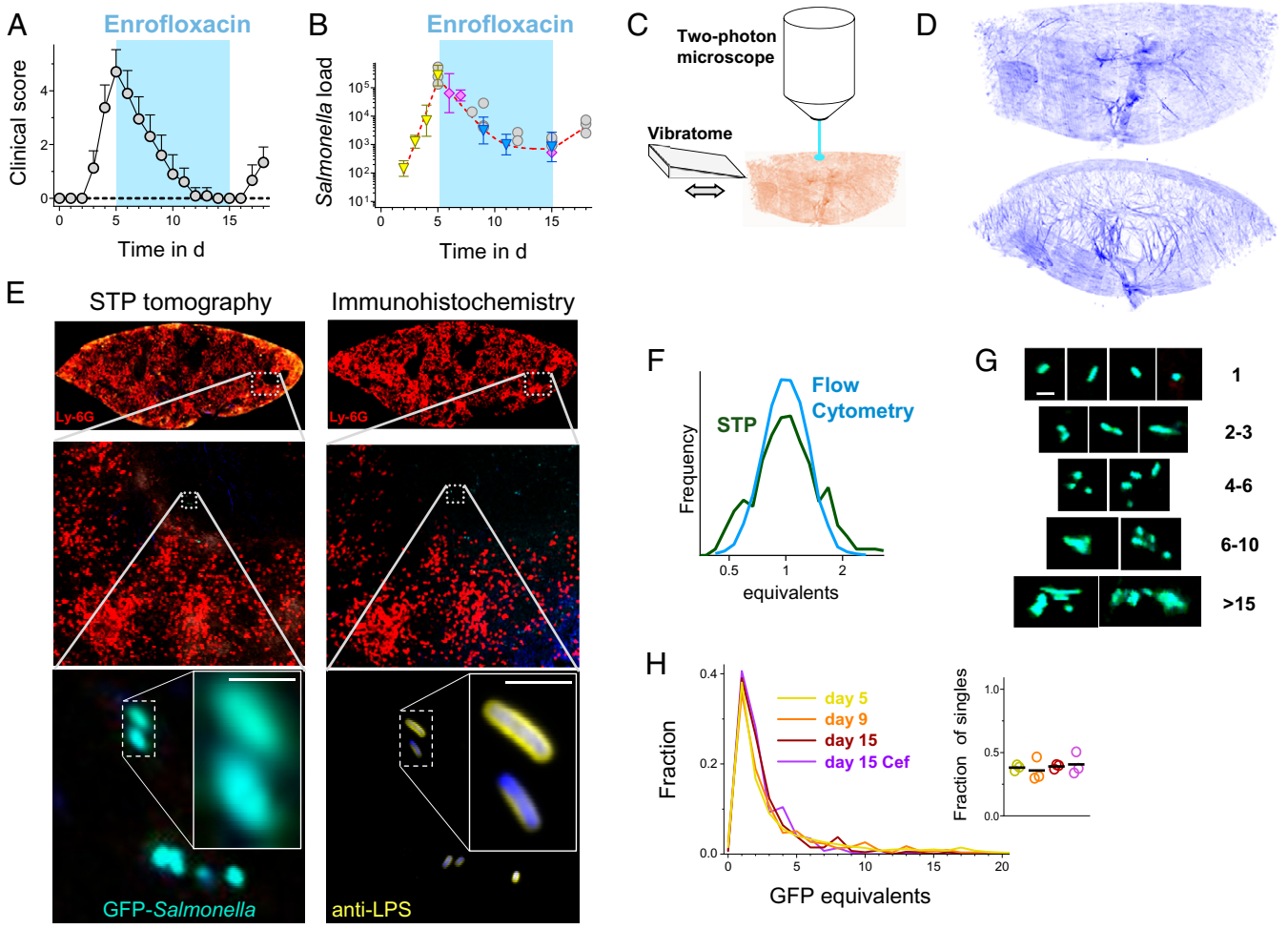

Fig. 1. Spleen-wide monitoring of *Salmonella* survival during antimicrobial chemotherapy. (*A*) Disease scores of orally infected mice. From day 5 to day 14, mice received daily 5 mg/kg enrofloxacin. Arithmetic means and SDs are shown for 3 to 26 mice. (*B*) *Salmonella* loads in the spleen of orally infected mice as determined by plating (triangles), flow cytometry (diamonds), or serial two-photon tomography (circles). Plating and flow cytometry results are shown as geometric means and SDs for groups of 3 to 20 mice (yellow labels indicate previously reported values) (42). Each tomography data point represents an individual mouse. The dashed line from days 2 to 5 shows an exponential fit; the line from days 5 to 15 shows an exponential decay with *y* offset; and the line from days 15 to 18 connects the geometric means. (*C*) Principle of STP tomography. A vibratome removes the surface of a tissue block. A two-photon microscope scans the blockface, before the vibratome removes the next section. (*D*) Side and top views of collagen fibers (trabeculae) detected by STP tomography of a 5-mm spleen slice. (*E*) Detection of GFP-*Salmonella* by STP tomography in one optical section (*Left*). Neutrophils were stained by in vivo injection of a phycoerythrin-labeled Ly-6G antibody. Green fluorescent particles were confirmed by staining the corresponding vibratome section with an antibody to *Salmonella* LPS and imaging by confocal microscopy (*Right*). (Scale bars, 3 μm.) (*F*) GFP fluorescence intensity distribution of single *Salmonella* cells in the spleen at day 5 after oral infection as analyzed by flow cytometry (n = 7,685) or STP tomography (n = 681). Intensities were normalized to the respective median. (*G*) Examples of single *Salmonella* cells and microcolonies in the spleen as detected by STP tomography. The numbers on the *Right* represent estimates for the number of *Salmonella* cells based on total GFP fluorescence. (Scale bar, 5 μm.) (*H*) Size distributions of *Salmonella* objects in orally infected mice before (day 5) and during antimicrobial chemotherapy. The data represent pooled data from three mice per group and 39 to 362 *Salmonella* objects per mouse. The *Inset* shows the fraction of single *Salmonella* among all *Salmonella* objects with each circle representing an individual mouse.

that ~40% of *Salmonella* resided alone with no conspecifics in their immediate (<5 μm) neighborhood consistent with previous findings (55, 56) (Fig. 1*H*). Based on number and size of microcolonies and the imaged tissue volume, we estimated the total number of *Salmonella* cells per spleen. These data were consistent with plating results and flow cytometry of independently infected mice (Fig. 1*B*). Thus, STP tomography reliably localized and quantified individual *Salmonella* cells at population densities down to one cell in 100 mm^3 tissue.

Comparison of *Salmonella* objects before and after 10 d of chemotherapy with either enrofloxacin or ceftriaxone revealed unaltered microcolony-size distributions. We did not detect a preferential survival of isolated single *Salmonella* cells during antimicrobial clearance of 99% of all *Salmonella*, which was inconsistent with the proposed exclusive survival of single nonreplicating *Salmonella* persister cells (57).

Antimicrobial Clearance of *Salmonella* Is Ineffective in the Splenic WP. STP tomography enabled us to localize scarce surviving *Salmonella* during antimicrobial chemotherapy at the whole-organ level. The spleen has three major compartments with distinct physiological functions (58): the red pulp (RP) that serves as a blood reservoir and removes aged erythrocytes; the WP containing high densities of B and T lymphocytes for inducing adaptive immunity to bloodborne pathogens; and the intermittent marginal zone (MZ) that captures bloodborne particles and pathogens. We identified these three regions by in vivo staining of CD169 (also called Siglec-1 or Sialoadhesin), a marker for a macrophage subtype in the MZ (59) (Fig. 2 *A* and *B*). We noticed that *Salmonella* clearance kinetics in RP resembled those in the MZ. We, therefore, combined data for these two compartments (RP/MZ) and compared them with those for WP.

Before treatment, ~95% of the ~200,000 *Salmonella* cells resided in RP/MZ (60, 61) (Fig. 2*C*). Enrofloxacin cleared *Salmonella* from these compartments with monophasic exponential kinetics with a rate of 0.44 ± 0.23 log per day for ~7 d, after which clearance decelerated markedly. After 10 d, ~300 *Salmonella* cells or ~0.15% of the initial load survived. By contrast, at start of therapy only ~10,000 (~5%) *Salmonella* cells resided in WP. Initial clearance of this minor *Salmonella* subset was 2-fold slower (0.21 ± 0.12 log per day) than in RP/MZ and decelerated markedly already after 4 d of treatment (day 9 postinfection, p.i.) with *Salmonella* loads declining less than 3-fold over the next 6 d. After a total of 10 d of treatment, ~1,000 *Salmonella* cells or ~10% of the initial load in the WP survived, a 70-fold larger fraction than in RP/MZ (Fig. 2 *C* and *D*).

Ceftriaxone, which differs from enrofloxacin by targeting peptidoglycan transpeptidases instead of DNA topoisomerases, and by lacking activity against nonreplicating bacteria (62–65), had similar inhomogeneous activity against *Salmonella* in the WP compared to RP/MZ (Fig. 2*D*), indicating that the diverging *Salmonella* survival did not depend on a particular antimicrobial mode of action or activity against nonreplicating bacteria.

Immunohistochemistry showed that surviving *Salmonella* in WP resided intracellularly in $CD68^+$ $Ly\text{-}6C^-$ $F4/80^-$ $CD21/35^-$ FDC^- $ER\text{-}TR7^-$ $gp38^-$ $CD3^-$ $CD19^-$ WP macrophages (59) at the boundary between T and B cell zones (Fig. 2*E*). We did not find *Salmonella* cells in B or T cells, follicular dendritic cells, dendritic cells, inflammatory monocytes, lymphatic epithelial cells, or reticular fibroblasts. Our data differ from previous studies that attempted to identify host cells of surviving *Salmonella* cells by analyzing tissue homogenates with flow cytometry. Homogenization disrupts most *Salmonella*-infected cells, even when done gently (55). Released bacteria can bind to other host cells in the tissue homogenate such as B cells (66), which do not harbor *Salmonella* in intact tissues (61).

Together, these data indicate that antimicrobial chemotherapy was particularly ineffective against a minor *Salmonella* population in WP.

Enrofloxacin Reaches the WP in Sufficient Amounts. The poor antimicrobial clearance of *Salmonella* from WP might reflect inefficient drug delivery (67). Enrofloxacin effectively penetrates tissues (64); however, the splenic WP receives blood solutes only by diffusion through a conduit system (68), in contrast to the direct blood supply to the RP/MZ (69). In addition, oral *Salmonella* infection caused extensive thrombosis in spleen veins (70) (Fig. 3*A*) that reduced blood circulation to and within the spleen as revealed by ultrasound imaging (Fig. 3 *B* and *C*).

To assess drug delivery, we isolated WP and RP/MZ using laser-capture microdissection (*SI Appendix*, Fig. S4*A*) and determined drug concentration with an enrofloxacin-specific ELISA. Enrofloxacin levels were slightly higher in RP/MZ than in WP but were >1 mg mL^{-1} at day 9 p.i. in both compartments (Fig. 3*D*), thus exceeding more than threefold the pharmacokinetic–pharmacodynamic target for effective bacterial killing (peak concentration: MIC ratio >12) (71–74). Killing assays with *Salmonella* cultures growing in chemostat cultures

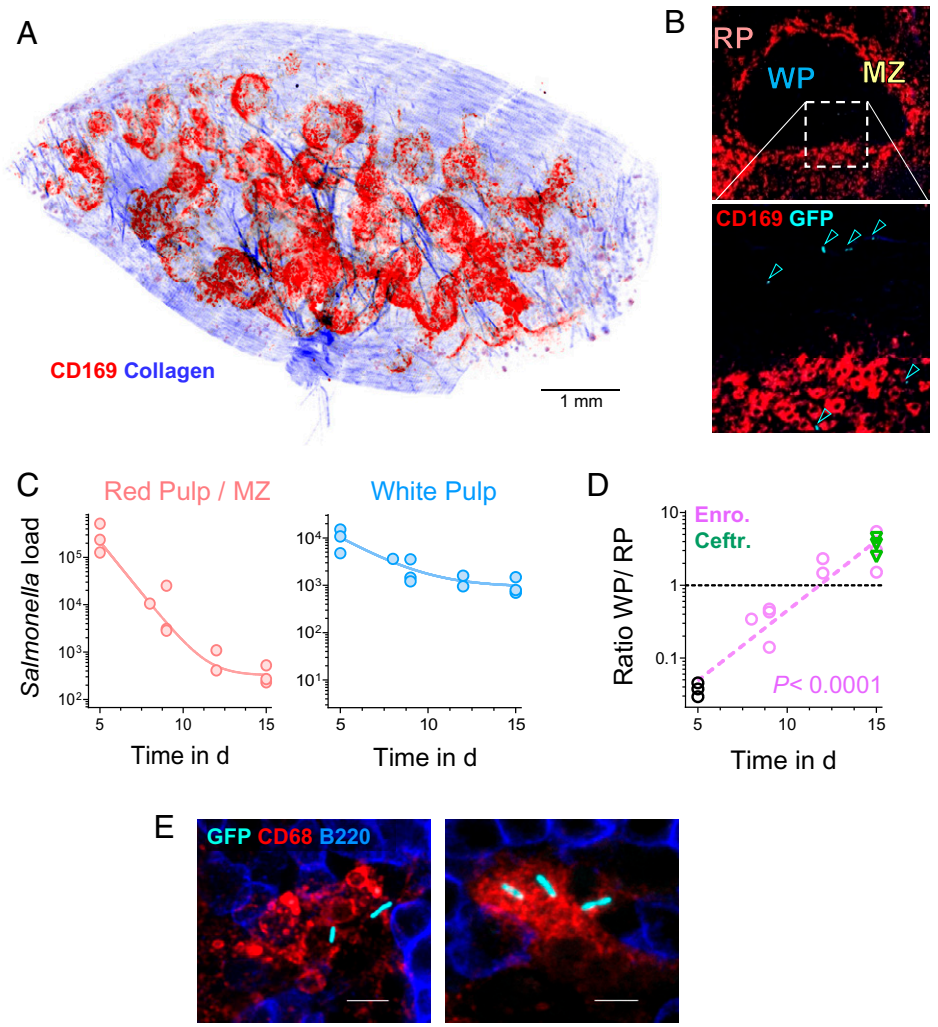

Fig. 2. Compartmentalized *Salmonella* clearance during antimicrobial chemotherapy. (*A*) Tomogram of a 5-mm spleen slice stained in vivo with an anti-CD169 antibody. (*B*) Localization of *Salmonella* cells (cyan, arrowheads) in spleen compartments (RP; MZ, marginal zone containing CD169-positive macrophages; WP) of an orally infected mouse. (*C*) *Salmonella* loads in spleen compartments of orally infected mice during enrofloxacin chemotherapy. Each circle represents STP data of an individual mouse. The lines are fits of monoexponential decays with *y* offsets. (*D*) Ratio of *Salmonella* loads in WP vs. RP/MZ during chemotherapy with enrofloxacin (Enro.; *P* value for deviation of slope from zero after linear regression of log-transformed data, shown as dashed line). Data for 10 d of treatment with ceftriaxone (Ceftr.) are also shown. Each symbol represents STP data of an individual orally infected mouse calculated from the data shown in *C*. (*E*) Localization of GFP-expressing *Salmonella* in CD68-positive macrophages at the periphery of B220-positive B cell zones in the splenic WP of orally infected mice after 10 d of treatment with enrofloxacin. (Scale bars, 5 μm.)

under in vivo mimicking conditions with generation times around 6 h (42) confirmed that enrofloxacin concentrations above 1 mg mL^{-1} caused saturated killing (*SI Appendix*, Fig. S4*B*) (73). Fluoroquinolones accumulate in phagocytes (75), suggesting even higher enrofloxacin exposure of *Salmonella* residing intracellularly in macrophages (Fig. 2*E*) compared to bulk average concentrations in the WP. These data suggested that sufficient drug was locally available for effective killing.

To track *Salmonella* killing by enrofloxacin in vivo, we treated mice at day 5 postinfection with enrofloxacin. Before administration and various times after, we killed mice and prepared spleen homogenates in detergent-containing buffer, which liberates >90% of all *Salmonella* from host cells and tissue fragments as a suspension of single bacteria (76). We sorted the *Salmonella* using flow cytometry and determined their survival by comparing CFUs on plates (live *Salmonella*) and flow cytometric counts (live and drug-killed *Salmonella*) (42). To ensure sufficient *Salmonella* numbers for rapid sorting, we used intravenously infected mice at day 5 postinfection (first enrofloxacin dose). *Salmonella* have indistinguishable replication rates and enrofloxacin susceptibility after oral or i.v. infection (42). The results show that enrofloxacin killed 90 to 95% of all *Salmonella* within the first hour (42) consistent with pharmacokinetic–pharmacodynamic target attainment (see above). However, little further killing occurred in the following 3 h (*SI Appendix*, Fig. S4*C*), consistent with results for chemostat cultures growing under in vivo mimicking conditions (*SI Appendix*, Fig. S4*D*) and reported in vitro data for enrofloxacin and other fluoroquinolones (74, 77). This biphasic killing is probably a consequence of a bacterial SOS response to fluoroquinolone exposure ("drug-induced tolerance") (77).

Overall, killing of slowly replicating *Salmonella* in mice and chemostats was rather limited compared to rapidly replicating bacteria in rich broth, where similar fluoroquinolone concentrations kill several logs of bacteria within 1 h of exposure (42, 74, 77). Killing activity of antibiotics against invasive *Salmonella* in human patients is also moderate (78, 79), and *Salmonella* with slightly reduced susceptibility to fluoroquinolones are associated with longer fever clearance times and increased risk of failure (37, 80), while other Enterobacterales with similarly decreased susceptibility can still be treated effectively (Clinical & Laboratory Standards Institute, CLSI, susceptibility breakpoints for ciprofloxacin: *Salmonella*, ≤0.06 μg/mL; other Enterobacterales, ≤0.25 μg/mL; http://em100.edaptivedocs.net/Login.aspx).

Enrofloxacin levels declined 5- to 10-fold in both RP/MZ and WP from 1 h to 4 h after drug administration (Fig. 3*D*), consistent

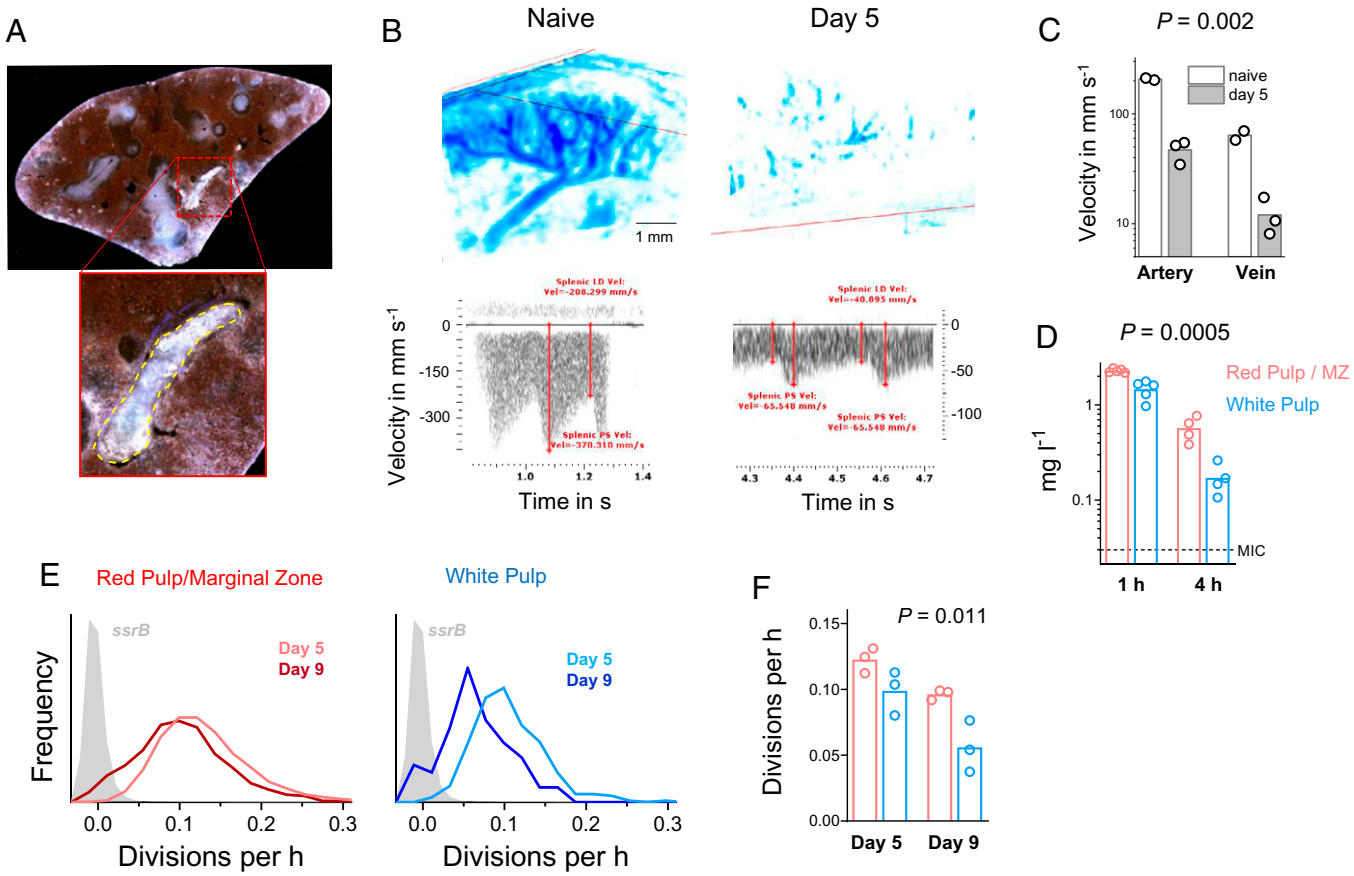

Fig. 3. Role of drug delivery and nonreplicating persisters. (*A*) Autofluorescence micrograph of a spleen section with a highly autofluorescent thrombus in a large vein. Similar images were obtained for all orally infected mice. (*B*) Ultrasound 3D power Doppler-mode images of blood flow in the spleen of naive and orally infected mice. (*Lower*) Corresponding blood flow velocities in the splenic artery as determined by pulsed-wave Doppler ultrasound. (*C*) Mean velocities in splenic arteries and veins of naive and orally infected mice. Each circle represents one mouse (repeated-measures two-way ANOVA comparing naive and infected mice). (*D*) Enrofloxacin concentration in different spleen compartments of orally infected mice. Each circle represents one mouse (repeated-measures two-way ANOVA comparing RP and WP). The MIC of enrofloxacin for the *Salmonella* strain as measured in Mueller–Hinton broth is shown for comparison. (*E*) *Salmonella* replication-rate distributions in different spleen compartments. The graphs represent pooled data for three orally infected mice per time point. The few nondividing *Salmonella* cells included enrofloxacin-killed *Salmonella* corpses that retain the $TIMER^{bac}$ protein. Previously reported in vivo data for the *ssrB* mutant, which shows a replication arrest in mouse spleen (42) are shown for comparison (gray). (*F*) Mean *Salmonella* division rates with each circle representing an individual orally infected mouse (*P* value: repeated-measures two-way ANOVA comparing red vs. white pulp).

with a terminal elimination half-life of enrofloxacin in mice in the range of 1 h (74, 81, 82). Progressively declining enrofloxacin levels will eventually stop enrofloxacin-mediated killing and even enable some *Salmonella* regrowth when enrofloxacin levels drop below the MIC (see below). Sub-MIC trough levels are known to occur for recommended doses in mice (74) (and occur also in human patients) (83) but are likely less problematic for treatment of more rapidly growing pathogens that are more efficiently killed by peak enrofloxacin levels early after administration of each dose. Indeed, the C_{max}/MIC ratio is a marker of effective treatment of various other pathogens with fluoroquinolones, while the fraction of time above the MIC is not (84). Higher or more frequent doses than recommended might reduce the fraction of time with sub-MIC enrofloxacin levels but would also increase adverse reactions (85).

Together, these results show pharmacokinetic–pharmacodynamic target attainment in both spleen compartments. Thus, insufficient drug delivery did not explain the sluggish *Salmonella* clearance from day 9 p.i. in WP. However, killing was mostly confined to the first hour after drug administration and overall rather limited because of *Salmonella's* low replication rates.

Surviving *Salmonella* Cells Continue to Replicate. It has been proposed that only nonreplicating *Salmonella* survive extensive antibiotic treatment in vivo (57). That study used continuous administration of enrofloxacin doses that were 30-fold higher than recommended for rodents. *Salmonella* viability after treatment was assessed indirectly based on fluorescence changes upon tissue lysis with detergent and incubation in rich medium. The observed ∼65% fluorescence decline could reflect dilution of preloaded GFP by one to two *Salmonella* divisions during the 12-h incubation, which was taken as evidence for viability (57), but the data do not exclude partial GFP leakage from damaged *Salmonella* corpses as an alternative interpretation. Two other studies did not detect any viable colony-forming *Salmonella* under identical experimental conditions (42, 45), suggesting that the nonreplicating *Salmonella* particles are largely nonviable posttreatment. Other studies suggested survival of slowly replicating *Salmonella* in mice treated with more clinically relevant doses of fluoroquinolones (44, 86).

To determine the replication status of surviving *Salmonella* in our model, we used STP tomography to quantify fluorescence of *Salmonella* expressing TIMER^{bac}, a reporter protein with differential maturation kinetics of green and orange fluorophores. The green-to-orange fluorescence ratio depends on the overall protein dilution associated with bacterial growth and division and thus indicates the single-cell replication rate (42). TIMER^{bac} data for *Salmonella* in infected mice are consistent with independent measurements of in vivo replication rates based on dilution of a nonreplicating plasmid. TIMER^{bac} data are also consistent with net growth of *Salmonella* wild-type (WT) and attenuated mutants in mouse lines with differential resistance to *Salmonella* infection (42, 87). STP tomography of TIMER^{bac}-*Salmonella* revealed heterogeneous replication rates (42) that were higher in RP/MZ than in WP. Median rates at 24 h after the last enrofloxacin dose declined during treatment in both compartments because of preferential killing of fast dividing subsets (42) (Fig. 3 *E* and *F*). However, the majority of *Salmonella* cells in both compartments continued to divide, consistent with sub-MIC trough levels (see above), and TIMER^{bac} patterns remained distinct from those of a *ssrB* mutant, which shows replication arrest after a few initial divisions in vivo (42, 88). This was even true at day 9 p.i., when clearance essentially stopped in WP (Fig. 2*C*). The few "nondividing" *Salmonella* cells included enrofloxacin-killed *Salmonella* corpses with lethal DNA damage but intact envelopes retaining the TIMER^{bac} protein (42). Ongoing *Salmonella* replication was also supported by direct observation of dividing cells after 10 d of treatment in tissue sections (day 15 p.i.; Fig. 2*E* and *SI Appendix*, Fig. S5). Moreover, we did not detect any preferential survival of isolated single *Salmonella* cells during clearing of 99.5% of all bacteria (Fig. 1*H*). Together, these data indicated that replication arrest was not a critical factor of *Salmonella* survival during treatment.

Host-Imposed Stresses Have Minor Impact on *Salmonella* Survival. Host-imposed stresses, such as reactive oxygen species (ROS) and nitric oxide (NO), can promote bacterial tolerance to antibiotics (7–13). *Salmonella* are exposed to diverse stresses in infected spleen that are highly heterogeneous at the single-cell level (89). This heterogeneity provides unique opportunities to compare directly *Salmonella* subsets with high or low stress in the same host tissue in terms of their antimicrobial susceptibility. To test this idea, we infected mice with various *Salmonella* stress-reporter strains. At day 5 postinfection, we administered enrofloxacin and 1 h later, we prepared detergent-treated spleen homogenates to release >90% of all *Salmonella* from host cells and tissue fragments as a suspension of single bacteria (76). We sorted stressed and nonstressed *Salmonella* subsets using flow cytometry and determined their survival by comparing CFUs on plates (live *Salmonella*) and flow cytometric counts (live and drug-killed *Salmonella*) (42) (Fig. 4*A*). To ensure sufficient *Salmonella* numbers for rapid sorting, we used intravenously infected mice at day 5 (first enrofloxacin dose). *Salmonella* have indistinguishable replication rates and enrofloxacin susceptibility after oral or i.v. infection (42).

The results showed that a ∼10% of the *Salmonella* subpopulation with high P_{katG}-*gfp* activity indicating exposure to host-derived ROS (61), survived enrofloxacin approximately twofold better than GFP^{low} *Salmonella* with low oxidative stress (Fig. 4 *A* and *B* and *SI Appendix*, Fig. S6*A*). *Salmonella* required *acrB*, but not *katG*, for this protective effect, suggesting that host ROS antagonized enrofloxacin activity by stimulating AcrB-mediated drug efflux (90) and not by altering redox physiology (61, 91).

Salmonella cells with high P_{hmpA} activity indicating exposure to host-derived NO (61), had ∼1.5-fold lower survival than nonexposed *Salmonella* (Fig. 4*B* and *SI Appendix*, Fig. S6*B*). A *Salmonella* mutant ("Δ4," Δ*hmpA* Δ*hcp-hcr* Δ*ytfE*) with detoxification defects that increase the NO concentration in exposed bacteria (61), had similar survival patterns. Thus, physiological NO may not increase killing itself, but rather represent a marker for microenvironments that enhance enrofloxacin activity.

Salmonella cells with high $P_{phoP\text{-}1}$ (92) activities had ∼2.5-fold lower survival than cells with low $P_{phoP\text{-}1}$ activity (Fig. 4*B* and *SI Appendix*, Fig. S6*B*). $P_{phoP\text{-}1}$ correlated with *Salmonella* replication rate (*SI Appendix*, Fig. S4*C*), which is associated with increased enrofloxacin susceptibility in vivo (42) (Fig. 4*B*). However, monitoring replication rate and $P_{phoP\text{-}1}$ activity together revealed an additional ∼2-fold replication-independent effect of high $P_{phoP\text{-}1}$ activity (Fig. 4*B* and *SI Appendix*, Fig. S6*D*). Thus, microenvironments that stimulate $P_{phoP\text{-}1}$ enhance enrofloxacin activity through both replication-promoting and replication-independent factors. Neither low magnesium nor low pH, stimuli known to induce $P_{phoP\text{-}1}$ (93), are likely to be associated with enhanced enrofloxacin activity, because the magnesium-nonresponsive *Salmonella phoQ* H157R mutant (94) showed similar killing patterns, and low pH diminished enrofloxacin activity (MIC values: pH 7.4, 0.03 mg per liter; pH 5.5, 0.06 mg per liter; pH 5.0, 0.24 mg per liter). Antimicrobial peptides, which also induce $P_{phoP\text{-}1}$ (93), can promote antibiotic action (95) but testing their role in mice is difficult because the only described antimicrobial peptide-nonresponsive *Salmonella* mutant has additional signaling defects (96).

Together, these data showed complex modulation of *Salmonella* susceptibility by heterogeneous host-imposed stresses.

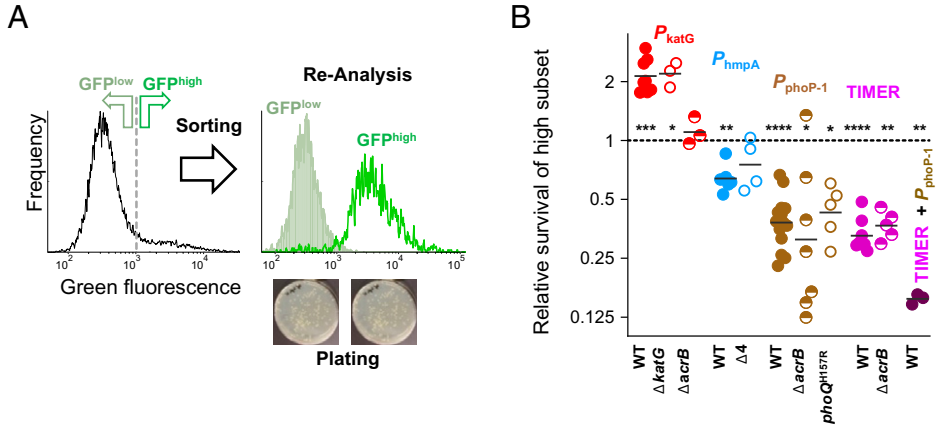

Fig. 4. Role of stress-induced tolerance. (*A*) Strategy for determining survival of stressed *Salmonella* subsets during chemotherapy of intravenously infected mice. *Salmonella* carrying a GFP-reporter plasmid for oxidative stress show heterogeneous fluorescence in the spleen at 1 h (*Left*) (61). This signal is not affected by 1 h of in vivo enrofloxacin exposure or various mutations (*SI Appendix*, Fig. S6). GFP^{low} and GFP^{high} subsets are sorted and survival rates are determined by comparing flow cytometry counts (live and dead *Salmonella*) with plate counts (live *Salmonella*). (*B*), Relative survival of *Salmonella* subsets for different reporter constructs and *Salmonella* genotypes. Each symbol represents an individual i.v. infected mouse (*$P < 0.05$; **$P < 0.01$; ***$P < 0.001$; ****$P < 0.0001$; one-sample *t* test of log-transformed data with Holm–Šídák correction for multiple comparisons).

However, effect sizes were moderate and some of the stresses were actually associated with enhanced antibiotic activity, arguing against host stresses as a critical factor supporting *Salmonella* survival during antimicrobial chemotherapy.

Declining Inflammation Diminishes *Salmonella* Clearance. *Salmonella* infection triggers an inflammatory host response with infiltration of neutrophils and inflammatory monocytes. These cells kill *Salmonella* by oxidative damage (61, 97, 98) and envelope disruption (99), which partially controls disease progression (100, 101). Host inflammation supports antimicrobial clearance of bacteria (44, 66, 102–107) and may thus be a relevant factor influencing *Salmonella* survival.

Inflammation was not constant during treatment. Instead, various parameters all showed declining inflammation: clinical symptoms resolved during chemotherapy (Fig. 1*A*) together with declining serum concentrations of the inflammatory cytokine IFNγ (*SI Appendix*, Fig. S7*A*). In the spleen, infiltration by neutrophils and inflammatory monocytes (Fig. 5 *A* and *B*) and the abundance of inflammation-associated transcripts *Ifng*, *Tnfa*, and *Mpo* all declined (Fig. 5*C*). A similar decline in inflammation has previously been observed during high-dose ciprofloxacin treatment of a *Salmonella*-enteritis mouse model (44).

In addition, inflammation was also inhomogeneous across spleen compartments with markedly higher neutrophil densities and transcript abundance in RP/MZ than in WP (Fig. 5 *A*–*C*). In particular, abundance of *Mpo* transcripts, a marker for neutrophils and inflammatory monocytes, dropped >1,000-fold in WP from days 5 to 9 p.i., consistent with the local depletion of these cell types as observed by immunohistochemistry. These data showed inhomogeneous and declining inflammation during antimicrobial chemotherapy, probably in response to local *Salmonella* loads (100, 108–110). In particular, inflammation was already weak at the start of treatment in the WP, which was scarcely colonized by *Salmonella*, and declined in both compartments with falling *Salmonella* loads.

Comparison of the spatiotemporal inflammation dynamics and *Salmonella* clearance indicated that at times and places with low neutrophil and monocyte densities, clearance was particularly inefficient. An important role of neutrophils and monocytes was confirmed by antibody-mediated depletion of these cells, which further impaired *Salmonella* clearance (66) (*SI Appendix*, Fig. S7*B*). These data suggested that the fading support from neutrophils and other inflammatory processes during treatment might have caused diminishing clearance rates and eradication failure.

To test this idea, we aimed at delaying the decline of inflammation. We coinfected mice orally with a GFP-*Salmonella* WT strain (MIC, 0.03 μg/mL) and a YFP-*Salmonella* enrofloxacin-resistant (ER) strain with decreased susceptibility (MIC, 0.25 μg/mL, which is still below the CLSI enrofloxacin susceptibility breakpoint of ≤0.5 μg/mL, http://clsivet.org/Login.aspx). The ER strain should be cleared more slowly during chemotherapy because of its decreased susceptibility, thus maintaining stimulation for inflammatory responses, while the WT strain would enable monitoring the clearance of susceptible *Salmonella* under these conditions. At the start of treatment (day 5 p.i.), mice infected with the strain mixture had similar *Salmonella* loads and clinical scores compared to mice infected with WT alone (Fig. 5*D* and *E*). Enrofloxacin treatment cleared YFP-*Salmonella* ER less efficiently than WT in single-strain infections as predicted, and this was associated with a slower decline of disease symptoms (Fig. 5 *D* and *E*), serum IFNγ (*SI Appendix*, Fig. S7*A*), neutrophil and monocyte infiltration, and inflammation-associated transcripts (Fig. 5 *A*–*C*).

In the presence of this sustained inflammation, antimicrobial chemotherapy successfully eradicated the coinfecting susceptible WT strain, in marked contrast to the GFP-WT single-strain infections where *Salmonella* eradication was impossible (Fig. 5*D*). This supported the idea that the declining contribution of neutrophils and monocytes to *Salmonella* clearance caused treatment failures. *Salmonella* ER maintained high loads under the same conditions, suggesting that their approximately eightfold lower sensitivity to enrofloxacin resulted in poor clearance even with sustained inflammation support. Treatment failures occur also in human patients infected with *S. enterica* serovar Typhi strains with moderately decreased susceptibility to fluoroquinolones (37, 111).

Direct competition between ER and WT *Salmonella* strains did not explain the accelerated clearance of WT in mixed infections, because the two strains did not coinfect the same host cells but remained separated by several noninfected cells (Fig. 5 *F*–*H*) consistent with clonal spreading of infection foci without mixing (56). Limited inter-*Salmonella* competition in the spleen was supported by unchanged *Salmonella* single-cell replication rates across a hundredfold changes in *Salmonella* tissue loads during acute infection (42) and the comparable *Salmonella* loads in mixed vs. single-strain infections at day 5 (Fig. 5*D*).

Our data are in general agreement with previous observations that stimulating inflammation can reduce antibiotic persistence of *Salmonella* in a mouse enteritis model (44). However, in our model injection of killed *Salmonella* or purified lipopolysaccharide (LPS) did not accelerate *Salmonella* clearance of the susceptible strain. Injected LPS is captured in the MZ (and other organs) with limited spread to splenic RP and WP (112, 113), which might limit its impact on locally persisting *Salmonella*.

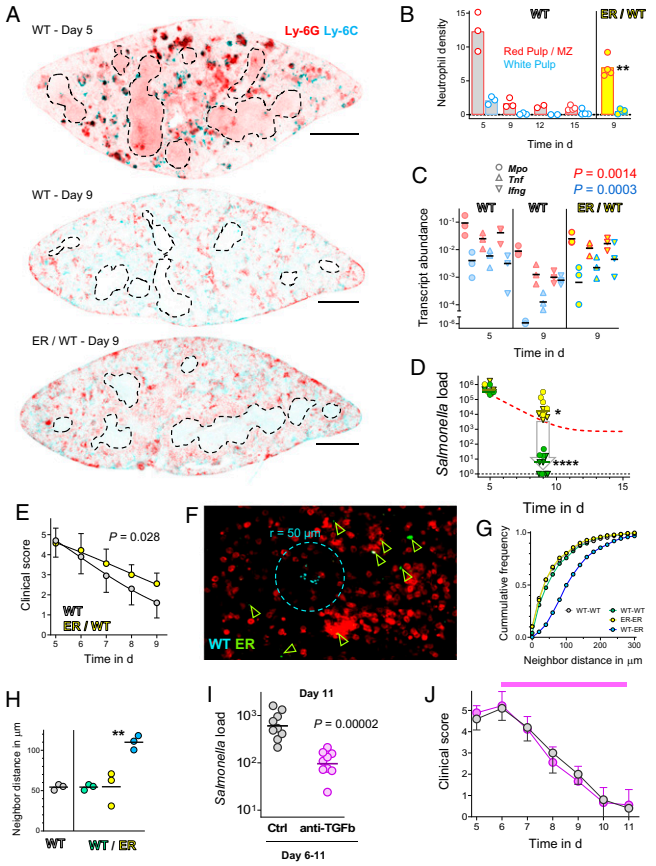

Fig. 5. Inhomogeneous and declining inflammation impairs *Salmonella* clearance. (*A*) Immunohistochemistry of spleen sections of mice orally infected with WT *Salmonella* or mixtures of wild-type and enrofloxacin-resistant *Salmonella* (ER/WT). Enrofloxacin treatment commenced at day 5. Ly-6G stains neutrophils and Ly-6C stains inflammatory monocytes. Fluorescence micrographs were inverted for improved visibility. (Scale bars, 1 mm.) (*B*) Neutrophil density at different time points after oral infection. Each symbol represents an individual orally infected mouse. The bars represent means (**$P < 0.01$; two-way ANOVA for single-strain vs. mixed infections at day 9). (*C*) Transcript abundance in different spleen compartments (red, RP/MZ; blue, WP) of mice infected with WT *Salmonella* or mixtures of WT and enrofloxacin-resistant *Salmonella* (ER/IR). Each symbol represents an orally infected mouse (two-way ANOVA for comparison of log-transformed data for single vs. mixed infections at day 9). (*D*) *Salmonella* loads in the spleen at various time points after oral infection with mixtures of WT and ER *Salmonella*. The dashed red line represents the fit for mice infected only with WT *Salmonella* shown in Fig. 1*B*. Enrofloxacin treatment commenced at day 5. Each symbol represents an individual mouse (circles, data from STP tomography; triangles, plating results; *$P < 0.05$; ****$P < 0.0001$; one-way ANOVA of log-transformed data with Holm–Šídák correction for multiple comparisons). (*E*) Clinical scores of mice infected orally with only WT *Salmonella* (same data as shown in Fig. 1*A*), or mixtures of wild-type and enrofloxacin-resistant *Salmonella* (ER/WT), during enrofloxacin chemotherapy (mixed-effect analysis with Geisser–Greenhouse correction). (*F*) Serial two-photon micrograph of a spleen from a mouse at day 5 after oral infection with a mixture of wild-type (WT, GFP) and enrofloxacin-resistant (ER, YFP) *Salmonella*. (*G*) Distribution of distances to nearest neighbors of the same or another *Salmonella* strain at day 5 after oral infection with WT *Salmonella* or mixtures of WT and enrofloxacin-resistant *Salmonella* (ER/IR). Data were pooled form three mice per group. (*H*) Median nearest neighbor distances for comparisons shown in *G*. Each symbol represents an orally infected individual mouse (**$P < 0.01$ for comparison of WT-ER vs. all other groups; one-way ANOVA with Holm–Šídák correction for multiple comparisons). (*I*) Impact of adjunctive therapy with a neutralizing antibody to TGFβ or an isotype antibody (Ctrl.) on *Salmonella* tissue loads after 6 d of treatment with enrofloxacin and adjunctive anti-TGFβ therapy for the last 5 d. Each symbol represents CFU data from an orally infected mouse (*t* test of log-transformed data). (*J*) Clinical scores of mice shown in *I*. The magenta line indicates the anti-TGFβ treatment (enrofloxacin started at day 5).

In a complementary experiment, we determined *Salmonella* clearance at low *Salmonella*, neutrophil, and monocyte densities. For this purpose, we already started chemotherapy on day 1 p.i., when *Salmonella* loads were still low, neutrophils and inflammatory monocytes still scarce (*SI Appendix*, Fig. S7 *C* and *D*), and clinical symptoms absent. We used intravenous infection for these experiments to reduce experimental variation. Early-onset enrofloxacin treatment prevented disease progression but failed entirely to reduce *Salmonella* loads (*SI Appendix*, Fig. S7*E*). *Salmonella* surviving 3 d of treatment had indistinguishable replication rates compared to start of treatment (*SI Appendix*, Fig. S7*F*), again arguing against a relevant role of nonreplicating cells.

In in vitro cell-culture infections, *Salmonella* survival of antimicrobial chemotherapy requires the type III secretion system 2 (T3SS-2) and the T3SS-2 effector protein SteE/SarA to induce an antiinflammatory, M2-like polarization of the infected macrophage (114). By contrast, early-onset treatment in infected mice was similarly ineffective for WT *Salmonella*, *Salmonella* Δ*ssrB* defective for T3SS-2, and *Salmonella* Δ*steE* (*SI Appendix*, Fig. S7*G*), indicating that neither T3SS-2 activity nor SteE/SarA is required for antibiotic persistence in vivo. *Salmonella* cell-culture infections differ fundamentally from the in vivo situation in various aspects (115), including the dominance (in vitro) vs. almost complete absence (in vivo) of nonreplicating persisters (42). The mutant phenotypes also suggest mechanistic differences between *Salmonella* in vivo survival during chemotherapy and *Salmonella* persistence in chronic infections (which requires SteE/SarA) (116), consistent with other differences in host cell types (Fig. 2*E*) (116, 117) and *Salmonella*-control mechanisms (antibiotic vs. CD4 T lymphocytes and TNFα) (102, 116, 118).

Together, these data show that *Salmonella* are efficiently cleared with sustained contributions from neutrophils and other inflammatory mediators, but not without such contributions. Thus, the always weak inflammation in WP and the further decline of inflammation during antimicrobial chemotherapy was the main cause of diminishing clearance rates and *Salmonella* persistence. Uneven drug delivery, nonreplicating persisters or slowly growing *Salmonella* subsets, stress-induced tolerance, and immunomodulatory capabilities of *Salmonella* must all have limited impact, because none of these factors could prevent *Salmonella* clearance when sustained inflammation supported chemotherapy. This was consistent with our direct analysis of these factors (see above).

Adjunctive Immunotherapy Safely Facilitates *Salmonella* Clearance. Maintaining inflammation during chemotherapy using continuous bacterial stimulation was effective for eradication of susceptible *Salmonella*. However, stimulation at this level was also associated with prolonged clinical symptoms, which would be unacceptable for improving patient treatment. A previous study found reduced antibiotic persistence of *Salmonella* in mice treated with lipopolysaccharide or CpG nucleotides (44) but these reagents have also unacceptable safety liabilities. More targeted interventions might disconnect the supportive role of some inflammatory responses from exacerbating disease symptoms. One possibility could be targeting the major cytokine TNFα, which plays a key role in *Salmonella* control during acute infection. However, TNFα has apparently no impact on antimicrobial clearance of *Salmonella* (102).

To identify more effective and safe adjunctive therapies, we considered that infiltrating neutrophils and inflammatory monocytes, which capture and destroy *Salmonella*, provided a major contribution to antimicrobial clearance of *Salmonella* (Fig. 5 *A*–*C*). We aimed at stimulating neutrophil functions using strategies with favorable safety profiles that are currently in clinical development as adjunctive cancer therapies. Specifically, we inhibited the suppressive effect of TGFβ on neutrophil function (119) using a

neutralizing antibody. TGFβ inhibition is currently under clinical development (120). We also tested IL-15 superagonist, an IL-15 complex with improved pharmacokinetics, to stimulate the natural killer cell/neutrophil axis that leads to superior antimicrobial properties of neutrophils (121). Various formulations of IL-15 are under active clinical development (122). We observed that both anti-TGFβ and IL-15 superagonist accelerated antimicrobial clearance of *Salmonella* by 85 to 95% (Fig. 5*I* and *SI Appendix*, Fig. S8*A*), without exacerbating or prolonging clinical symptoms (Fig. 5*J* and *SI Appendix*, Fig. S8*B*). Thus, safe adjunctive immunotherapies facilitate chemotherapy of difficult-to-treat *Salmonella* infections.

Discussion

In this study, we developed STP tomography to localize and characterize scarce *Salmonella* cells in whole host organs. Using this approach, we discovered that a minor *Salmonella* subset in the splenic WP survives antimicrobial chemotherapy orders of magnitude better than the *Salmonella* bulk population. Common assumptions could not explain this observation: the antibiotic reached the WP in sufficient amounts, *Salmonella* continued to replicate, and host stress-induced drug tolerance of *Salmonella* and *Salmonella*'s immunomodulatory capabilities had only minor impact. These findings demonstrate that concepts derived from laboratory models of bacterial persistence may have limited relevance for in vivo conditions in complex host tissues.

Instead, antimicrobial clearance of *Salmonella* required support of inflammatory cells such as neutrophils and monocytes, in part because antibiotics have poor activity in vivo against slowly replicating *Salmonella* in mice (42). Infiltration of neutrophils and monocytes followed local *Salmonella* density, which was high in the RP and MZ but low in the WP (this *Salmonella* tropism might reflect the low abundance of target phagocytes) (61). While large numbers of neutrophils and monocytes supported continuous antimicrobial clearance from RP and MZ until late in the treatment, the low and declining number of such cells in the WP supported only slow clearance over a few days. Eventually, local *Salmonella* numbers went below the threshold of pathogen-associated molecular patterns to recruit inflammatory cells and, therefore, the bacteria largely evaded killing but survived and replicated slowly. The critical role of inflammatory cell infiltration was confirmed by adjunctive therapies sustaining inflammation, which enabled successful eradication. Thus, complex tissue architecture, *Salmonella* tropism, and associated spatiotemporal host–pathogen dynamics determined success and failure of antimicrobial chemotherapy in vivo. These mechanisms required high-resolution, large-scale tissue imaging for discovery and would be difficult to reproduce under laboratory conditions.

The crucial role of host immunity for the outcome of antimicrobial chemotherapy is also revealed by previous studies with mouse strains that are genetically resistant to *Salmonella* infection. Although 10 or 12 days of treatment with clinically relevant doses of ciprofloxacin fail to eradicate *Salmonella* from spleen and liver (as for susceptible mice), resistant mice can control the surviving *Salmonella* without relapsing disease (39, 123). As many as 8% of humans in endemic areas for typhoid fever carry *Salmonella* in liver, gall bladder, and/or gall stones without showing typhoid disease symptoms (124–126), suggesting persisting but controlled infection. It is thus possible that some human typhoid fever patients show clinical cure despite microbiological eradication failure similar to what is observed in genetically resistant mice. Eradication failures that lead to clinically detected disease relapses might happen more frequently in patients with weak immunity. This could be tested in future clinical studies.

Our results show that STP tomography is a robust method to track and characterize scarce, micrometer-sized pathogen cells in their whole-organ host context. We focused our analysis on spleen but observed surviving *Salmonella* survivors also in Peyer's patches, mesenteric lymph nodes, and liver. All these reservoirs might contribute to relapses. The immediate increase of *Salmonella* in the spleen following treatment discontinuation in our model suggests local regrowth, but we cannot rule out migration between different sites. STP can be used to analyze all relevant organs, opening opportunities to identify and compare host microenvironments of surviving *Salmonella* and *Salmonella* fates during relapse in anatomically and functionally diverse tissues.

However, STP has also important limitations. The optical resolution of two-photon microscopy prevents detection of individual microbial cells within microcolonies. Currently available light-sheet systems still have inferior optical resolution for large tissues (127), but future improvements might ameliorate this issue. In vivo antibody staining can reveal surface-exposed epitopes in RP and MZ, but not intracellular structures or any epitopes in WP which excludes circulating antibodies in intact animals (68). Tissue-clearing methods enable antibody staining and visualization in permeabilized organs (127) and might be compatible with STP.

Our findings suggest opportunities to improve treatment of relapsing human invasive salmonellosis. In particular, adjunctive immune therapies that are already in clinical development for other medical indications, facilitated *Salmonella* clearance. Future studies might unravel optimal dosing of such therapies. Further insights into inflammatory mechanisms contributing to antimicrobial clearance of *Salmonella* could improve specific targeting with minimal adverse reactions. Our strategy and approaches might be applicable to elucidate mechanisms of bacterial persistence in other difficult-to-treat infections such as tuberculosis, which is also associated with heterogeneous bacterial colonization, slow but ongoing mycobacterial in vivo replication even after prolonged chemotherapy, poor activity of antimicrobials, and dynamically changing inflammatory responses (128).

Materials and Methods

Study Design. In this study, we developed a method, STP tomography, to study persisting *Salmonella* cells in infected animals. Mice were randomized for experiments comparing treatments. Investigators were not blinded to allocation during experiments and outcome assessment. However, tomography and flow cytometry were performed automatically. We estimated sample size by a sequential statistical design. We first infected two to three mice each based on effect sizes and variation observed in our previous studies (129), and used the results to estimate group sizes for obtaining statistical significance with sufficient power. The number of replicates is indicated where applicable.

***Salmonella* Strains.** *Salmonella* strains used in this study were based on *S. enterica* serovar Typhimurium SL1344 *hisG xyl* (130, 131). GFP- or YFP-expressing strains carried the fluorescent protein–encoding genes in the *sifB* locus that has homogenous high activity in vivo (55). TIMER^{bac} was expressed from the P_{ybaJ} promoter (132) on a low-copy episomal pSC101 derivative (42). Reporter strains carried pSC101 derivatives with constitutive expression of *mCherry* or *mtagbfp2* from the P_{ybaJ} promoter and transcriptional fusions of candidate promoters to *gfp-ova* coding for degradable fluorescent protein variants (half-life in the range of 30 min) (133). *Salmonella* mutants with gene deletions were obtained by two consecutive single crossovers with positive selection for resistance to kanamycin and negative selection for levan sucrase–mediated sensitivity to sucrose (134).

To mimic in vivo conditions, we cultured *Salmonella* in 100 mM 2-(N-morpholino)ethanesulfonic acid (MES), 5 mM KCl, 15 mM NH_4Cl, 0.5 mM K_2SO_4, 1 mM KH_2PO_4, 50 μM $MgSO_4$, 0.02% casamino acids, 0.02% glycerol, 0.0042% *N*-acetylglucosamine, 0.003% glucose, 0.0018% glucosamine, 0.005% histidine, 25 mM $NaHCO_3$, pH 5.5, and with a constant stream of 10% O_2/5% CO_2 in minichemostats (135) at a generation time of 6 h. Growth conditions were maintained for 72 h before addition of antibiotics.

Animals. We used 10- to 16-wk-old female BALB/c mice (Charles River Laboratories). Mice were housed in groups on a 12-h light/dark cycle in individually ventilated cages. The mice had ad libitum access to food and acidified drinking water. All animal experiments were approved (license 2239, Kantonales

Veterinäramt Basel) and performed according to local guidelines (Tierschutz-Verordnung, Basel) and the Swiss animal protection law (Tierschutz-Gesetz).

Age-matched, 10- to 16-wk-old female BALB/c mice (Charles River Laboratories) were deprived of food and water for 4 h and then infected orally with around 5×10^7 CFUs. At day 5 postinfection, 50 to 80% of mice showed clear symptoms of disease (score 4 or 5, see below). To minimize the impact of variable incubation times after oral infection, we analyzed only those diseased mice. For some experiments, mice were infected by tail vein injection of about 1,000 CFUs. Intravenously infected mice show less variation in *Salmonella* tissue loads between individual mice and thus require fewer experimental animals for detecting differences. No i.v. infected animals were excluded from analysis. *Salmonella* have indistinguishable replication rates, net growth, and enrofloxacin susceptibility in the spleen after oral or i.v. infection (42).The inoculum size was determined by plating for each infection.

Details of antibody injections, scoring of disease signs, and organ preparation are described in *SI Appendix, SI Materials and Methods*.

Flow Cytometry. The spleen was homogenized in ice-cold phosphate-buffered saline containing 0.2% Triton X-100. All samples were kept on ice until analysis. Large host cell fragments were removed by centrifugation at $500 \times g$ for 5 min. The supernatant contains more than 90% of the total *Salmonella* population as dispersed single cells (76). Relevant spectral parameters were recorded in a FACS Fortessa II equipped with 405-nm, 488-nm, and 561-nm lasers (Becton Dickinson), using thresholds on side scatter (SSC) to exclude electronic noise. Experimental details are described in *SI Appendix, SI Materials and Methods*.

Serial-Section Two-Photon Tomography. We embedded the fixed tissues in 5% oxidized agarose, which was freshly prepared by incubating type I agarose (Sigma-Aldrich, A0169) in 10 mM $NaIO_4$ (Sigma S1878) for 2 h. Tissues were covalently cross-linked to the agarose by a 2.5-h incubation in an excess of borohydride buffer (10 mM $NaBH_4$, Sigma-Aldrich 452882, in 50 mM borax, Sigma 221732/50 mM boric acid, Sigma B6768, at pH 9.0, stirred overnight at 4 °C to dissolve). Spleens infected with TIMER^{bac}-expressing *Salmonella* were embedded in nonoxidized 5% type I agarose (Sigma-Aldrich, A0169) without cross-linking to prevent alteration of TIMER^{bac} emission spectra. We imaged embedded tissues using a two-photon whole-organ tomograph (TissueCyte 1000, TissueVision). We cut physical sections every 50 μm (spleen), 20 μm (liver), or 30 μm (Peyer's patches and mesenteric lymph nodes) at a speed of 0.3 mm/s (0.05 mm/s for liver and noncross-linked spleen). After each sectioning, we imaged layers 20 and 30 μm (all tissues), 40 μm (all except liver), and 50 and 60 μm (spleen) below the blockface in three channels (blue channel: 450 to 500 nm; green channel: Chroma Technology ET510/20m, 500 to 520 nm for GFP and green TIMER^{bac} emission, inbuilt 500 to 560 nm for GFP/YFP; red channel: 560 to 650 nm) using 940 nm excitation laser light (Mai Tai eHP, Spectraphysics). We imaged with a resolution of 0.435 μm in *x* and *y* by using a 20× objective with numerical aperture (NA) 1.0 (Plan Apo, Zeiss 421452-9880-000).

We used the CIDRE method for retrospective illumination correction (53) for each channel and optical plane with further correction for imaging depth. Each imaged section was formed from 800-× 800-μm "tiles" with an *x/y* overlap of 10%. There was no overlap in *z*. Illumination-corrected tiles from the entire spleen scan were stitched based upon their expected position in the *x/y* tile grid (no registration was conducted at tile overlap regions) using the MATLAB-based software package, StitchIt (https://github.com/SainsburyWellcomeCentre/StitchIt) (136). We segmented GFP- and YFP-expressing *Salmonella* cells with supervised machine learning by training the MATLAB support-vector machine classifier based on blue and green channels for GFP and all three-color channels for YFP. To remove autofluorescence among particles classified as "YFP," we trained an eight-layer deep convolutional neural network constructed with the MATLAB layers function. All analyses were conducted using MATLAB 2017b and 2018b. The custom code is available through GitHub (https://github.com/BumannLab/Li_BumannLab_2020).

Immunohistochemistry. Fifty-micrometer-thick spleen sections retrieved from the TissueCyte were stored at −20 °C in cryoprotectant (300 g sucrose, 10 g polyvinyl-pyrrolidone 40, 400 mL ethylene glycol, 400 mL PB buffer (10 mM NaH_2PO_4, 40 mM Na_2HPO_4), after dissolving, PB buffer was added to 1 liter) (137). Sections were washed thrice for 5 min with Tris-buffered saline pH 7.4 (TBS). For antigen retrieval, sections were incubated in 5 mL prewarmed 10 mM sodium citrate, pH 8.5, at 37 °C for 45 min. Sections were washed thrice with TBST (0.1% Triton X-100 in TBS), blocked for 1 h with 1% BSA-fraction V, 2% mouse serum in TBST, and washed again thrice with TBST. Sections were incubated in 10 μg/mL primary antibody in TBST at 4 °C overnight, washed thrice with TBST, and stained with 10 μg/mL secondary antibody for 1 h at room temperature (antibodies are listed in *SI Appendix, SI Materials and Methods*). Sections were washed thrice with TBST and mounted in 70 μL mounting medium (Dako) and examined using a Leica SP8 confocal microscope.

Laser-Capture Microdissection, Enrofloxacin ELISA, and RT-PCR. Freshly prepared unfixed spleen was wrapped with aluminum foil and put into a 50-mL tube precooled in liquid nitrogen. Frozen spleen was stored at −80 °C. Frozen 50-μm-thick sections were cut at −14 °C with a cryotome (Leica, CM1950), placed on a PET FrameSlide (Zeiss, 415190-9101-000), and dried overnight in a 50-mL tube containing 10 mL silica gel orange (Sigma, 13767). Dried sections were cut with a laser-capture microdissection microscope (Zeiss PALM-Microdissection) with a 5× objective, 100% laser power, 68% focus, and three cut cycles. The area of all the cuts was recorded and summed. The cut pieces were collected using fine forceps under a macroscope (Olympus SZ60). Enrofloxacin was quantified with the MaxSignal Enrofloxacin ELISA test kit (Bioo Scientific 1017-01) and converted into concentration values based on corresponding microdissection areas and the section thickness of 50 μm.

For RT-PCR, frozen 50-μm-thick sections were cut at −14 °C with a cryotome (Leica, CM1950), placed on PET FrameSlide (Zeiss, 415190-9101-000), and stored in a 50-mL tube with 45 mL pure ethanol (Sigma, 1117271000). Before laser dissection, slides were taken out and put into a 1-L bottle containing 500 mL silica gel orange (Sigma, 13767) for 30 min. Dried sections were cut with a laser-capture microdissection microscope (Zeiss PALM-Microdissection) with a 5× objective, 100% laser power, 68% focus, and three cut cycles. Microdissected tissue was collected in TRIzol Reagent (Fisher Scientific, 15596026). RNA was extracted with a Quick-RNA Microprep kit (Zymo, R1050). RNA was reverse transcribed with a RT-PCT kit (Promega, A6010) and random oligonucleotide hexamers. cDNA was quantified with a real-time PCR system (Applied Biosystems StepOnePlus) using glyceraldehyde 3-phosphate dehydrogenase (GAPDH) as internal reference. The following oligos were used (*GAPDH*, TGTGTCCGTCGTGGATCTGA, CCTGCTTCACCACCTTCTTGAT; *Ifng*, AACGCTACACACTGCATCTTGG, GACTTCAAAGAGTCTGAGG; *Tnfa*, GGATACCAACTATTGCTTCAGCTCC, AGGCTCCAAATATAGGGGCAGGGTC; and *MPO*, TCCCACTCAGCAAGGTCTT, TAAGAGCAGGCAAATCCAG).

Ultrasound. Blood flow was measured in mice under isoflurane-anesthesia using Vevo3100 equipped with a MX550D transducer at 32 MHz (Visualsonics).

Quantification and Statistical Analysis. Statistical tests were performed with GraphPad Prism 8.0.2 as indicated in the figure legends. Error bars indicate mean ± SD unless otherwise noted. Statistical tests and associated *P* value are reported in *Results* or the figure legends. All statistical tests were two sided.

Data Availability. MATLAB code for analysis of SPT tomography data has been deposited in GitHub (https://github.com/BumannLab/Li_BumannLab_2020). All other study data are included in the article and supporting information.

ACKNOWLEDGMENTS. We are grateful to Sandra Meyer (Visualsonics) for help with ultrasound measurements, Wolf Heusermann (Biozentrum, Imaging Core Facility) for technical support in STP, and Frédéric Goormaghtigh (Biozentrum) and Guy Riddihough (Life Science Editors) for helpful comments. The work was supported by Swiss National Science Foundation 310030_156818 and 310030_182315 (to D.B.).

1. N. Q. Balaban *et al.*, Definitions and guidelines for research on antibiotic persistence. *Nat. Rev. Microbiol.* **17**, 441–448 (2019).
2. E. Bakkeren, M. Diard, W. D. Hardt, Evolutionary causes and consequences of bacterial antibiotic persistence. *Nat. Rev. Microbiol.* **18**, 479–490 (2020).
3. A. L. Moldoveanu, J. A. Rycroft, S. Helaine, Impact of bacterial persisters on their host. *Curr. Opin. Microbiol.* **59**, 65–71 (2021).
4. K. Lewis, The science of antibiotic discovery. *Cell* **181**, 29–45 (2020).
5. B. Prideaux, A. Lenaerts, V. Dartois, Imaging and spatially resolved quantification of drug distribution in tissues by mass spectrometry. *Curr. Opin. Chem. Biol.* **44**, 93–100 (2018).
6. L. Blanc *et al.*, High-resolution mapping of fluoroquinolones in TB rabbit lesions reveals specific distribution in immune cell types. *eLife* **7**, e41115 (2018).
7. D. A. Mitchison, The action of antituberculosis drugs in short-course chemotherapy. *Tubercle* **66**, 219–225 (1985).
8. K. Poole, Bacterial stress responses as determinants of antimicrobial resistance. *J. Antimicrob. Chemother.* **67**, 2069–2089 (2012).
9. J. H. Yang, S. C. Bening, J. J. Collins, Antibiotic efficacy-context matters. *Curr. Opin. Microbiol.* **39**, 73–80 (2017).
10. L. Radlinski, B. P. Conlon, Antibiotic efficacy in the complex infection environment. *Curr. Opin. Microbiol.* **42**, 19–24 (2018).

11. F. C. Fang, E. R. Frawley, T. Tapscott, A. Vázquez-Torres, Bacterial stress responses during host infection. *Cell Host Microbe* **20**, 133–143 (2016).
12. D. Bumann, O. Cunrath, Heterogeneity of Salmonella-host interactions in infected host tissues. *Curr. Opin. Microbiol.* **39**, 57–63 (2017).
13. J. E. Beam *et al.*, Macrophage-produced peroxynitrite induces antibiotic tolerance and supersedes intrinsic mechanisms of persister formation. *Infect. Immun.* **89**, e0028621 (2021).
14. R. H. Eng, F. T. Padberg, S. M. Smith, E. N. Tan, C. E. Cherubin, Bactericidal effects of antibiotics on slowly growing and nongrowing bacteria. *Antimicrob. Agents Chemother.* **35**, 1824–1828 (1991).
15. N. Sufya, D. G. Allison, P. Gilbert, Clonal variation in maximum specific growth rate and susceptibility towards antimicrobials. *J. Appl. Microbiol.* **95**, 1261–1267 (2003).
16. G. V. Smirnova, O. N. Oktyabrsky, Relationship between *Escherichia coli* growth rate and bacterial susceptibility to ciprofloxacin. *FEMS Microbiol. Lett.* **365**, fnx254 (2018).
17. N. Kaldalu, T. Tenson, Slow growth causes bacterial persistence. *Sci. Signal.* **12**, eaay1167 (2019).
18. M. H. Pontes, E. A. Groisman, A physiological basis for nonheritable antibiotic resistance. *MBio* **11**, e00817–e00820 (2020).
19. A. J. Lopatkin *et al.*, Bacterial metabolic state more accurately predicts antibiotic lethality than growth rate. *Nat. Microbiol.* **4**, 2109–2117 (2019).
20. B. Van den Bergh, M. Fauvart, J. Michiels, Formation, physiology, ecology, evolution and clinical importance of bacterial persisters. *FEMS Microbiol. Rev.* **41**, 219–251 (2017).
21. B. Gollan, G. Grabe, C. Michaux, S. Helaine, Bacterial persisters and infection: Past, present, and progressing. *Annu. Rev. Microbiol.* **73**, 359–385 (2019).
22. A. M. Cadena, S. M. Fortune, J. L. Flynn, Heterogeneity in tuberculosis. *Nat. Rev. Immunol.* **17**, 691–702 (2017).
23. Y. Shan *et al.*, ATP-dependent persister formation in *Escherichia coli*. *MBio* **8**, e02267–e02216 (2017).
24. B. B. Aldridge *et al.*, Asymmetry and aging of mycobacterial cells lead to variable growth and antibiotic susceptibility. *Science* **335**, 100–104 (2012).
25. E. H. Rego, R. E. Audette, E. J. Rubin, Deletion of a mycobacterial divisome factor collapses single-cell phenotypic heterogeneity. *Nature* **546**, 153–157 (2017).
26. T. Bergmiller *et al.*, Biased partitioning of the multidrug efflux pump AcrAB-TolC underlies long-lived phenotypic heterogeneity. *Science* **356**, 311–315 (2017).
27. Y. Wakamoto *et al.*, Dynamic persistence of antibiotic-stressed mycobacteria. *Science* **339**, 91–95 (2013).
28. H. Nicoloff, K. Hjort, B. R. Levin, D. I. Andersson, The high prevalence of antibiotic heteroresistance in pathogenic bacteria is mainly caused by gene amplification. *Nat. Microbiol.* **4**, 504–514 (2019).
29. F. Goormaghtigh, L. Van Melderen, Single-cell imaging and characterization of *Escherichia coli* persister cells to ofloxacin in exponential cultures. *Sci. Adv.* **5**, eaav9462 (2019).
30. D. Bumann, J. Fanous, J. Li, F. Goormaghtigh, Antibiotic chemotherapy against heterogeneous pathogen populations in complex host tissues. *F1000 Res.* **8**, 1781 (2019).
31. D. Shi, G. Mi, M. Wang, T. J. Webster, In vitro and ex vivo systems at the forefront of infection modeling and drug discovery. *Biomaterials* **198**, 228–249 (2019).
32. J. D. Stanaway, R. C. Reiner, B. F. Blacker, E. M. Goldberg; GBD 2017 Typhoid and Paratyphoid Collaborators, The global burden of typhoid and paratyphoid fevers: A systematic analysis for the Global Burden of Disease Study 2017. *Lancet Infect. Dis.* **19**, 369–381 (2019).
33. N. A. Feasey, G. Dougan, R. A. Kingsley, R. S. Heyderman, M. A. Gordon, Invasive non-typhoidal salmonella disease: An emerging and neglected tropical disease in Africa. *Lancet* **379**, 2489–2499 (2012).
34. M. A. Gordon *et al.*, Non-typhoidal salmonella bacteraemia among HIV-infected Malawian adults: High mortality and frequent recrudescence. *AIDS* **16**, 1633–1641 (2002).
35. T. Butler, Treatment of typhoid fever in the 21st century: Promises and shortcomings. *Clin. Microbiol. Infect.* **17**, 959–963 (2011).
36. J. A. Crump, M. Sjölund-Karlsson, M. A. Gordon, C. M. Parry, Epidemiology, clinical presentation, laboratory diagnosis, antimicrobial resistance, and antimicrobial management of invasive salmonella infections. *Clin. Microbiol. Rev.* **28**, 901–937 (2015).
37. C. N. Thompson *et al.*, Treatment response in enteric fever in an era of increasing antimicrobial resistance: An individual patient data analysis of 2092 participants enrolled into 4 randomized, controlled trials in Nepal. *Clin. Infect. Dis.* **64**, 1522–1531 (2017).
38. O. Rossi *et al.*, Within-host spatiotemporal dynamics of systemic Salmonella infection during and after antimicrobial treatment. *J. Antimicrob. Chemother.* **72**, 3390–3397 (2017).
39. H. Brunner, H. J. Zeiler, Oral ciprofloxacin treatment for Salmonella typhimurium infection of normal and immunocompromised mice. *Antimicrob. Agents Chemother.* **32**, 57–62 (1988).
40. D. J. Maskell, C. E. Hormaeche, Relapse following cessation of antibiotic therapy for mouse typhoid in resistant and susceptible mice infected with salmonellae of differing virulence. *J. Infect. Dis.* **152**, 1044–1049 (1985).
41. L. Bonina *et al.*, Beta-lactam antibiotics (aztreonam, ampicillin, cefazolin and ceftazidime) in the control and eradication of Salmonella typhimurium in naturally resistant and susceptible mice. *J. Antimicrob. Chemother.* **25**, 813–823 (1990).
42. B. Claudi *et al.*, Phenotypic variation of *Salmonella* in host tissues delays eradication by antimicrobial chemotherapy. *Cell* **158**, 722–733 (2014).
43. T. Ragan *et al.*, Serial two-photon tomography for automated ex vivo mouse brain imaging. *Nat. Methods* **9**, 255–258 (2012).
44. P. Kaiser *et al.*, Cecum lymph node dendritic cells harbor slow-growing bacteria phenotypically tolerant to antibiotic treatment. *PLoS Biol.* **12**, e1001793 (2014).
45. A. J. Griffin, L. X. Li, S. Voedisch, O. Pabst, S. J. McSorley, Dissemination of persistent intestinal bacteria via the mesenteric lymph nodes causes typhoid relapse. *Infect. Immun.* **79**, 1479–1488 (2011).
46. I. Arenas *et al.*, In vitro and in vivo antibiotic capacity of two host defence peptides. *Antimicrob. Agents Chemother.* **64**, e00145–e00120 (2020).
47. E. T. Arena *et al.*, Bioimage analysis of Shigella infection reveals targeting of colonic crypts. *Proc. Natl. Acad. Sci. U.S.A.* **112**, E3282–E3290 (2015).
48. M. R. Cronan *et al.*, Macrophage epithelial reprogramming underlies mycobacterial granuloma formation and promotes infection. *Immunity* **45**, 861–876 (2016).
49. C. Fung *et al.*, High-resolution mapping reveals that microniches in the gastric glands control Helicobacter pylori colonization of the stomach. *PLoS Biol.* **17**, e3000231 (2019).
50. W. Wang *et al.* Three-dimensional quantitative imaging of native microbiota distribution in the gut. *Angew. Chem. Int. Ed. Engl.* **133**, 3092–3098 (2021).
51. A. I. Ward *et al.*, *In vivo* analysis of Trypanosoma cruzi persistence foci at single-cell resolution. *mBio* **11**, e01242–e20 (2020).
52. M. Wendland, D. Bumann, Optimization of GFP levels for analyzing Salmonella gene expression during an infection. *FEBS Lett.* **521**, 105–108 (2002).
53. K. Smith *et al.*, CIDRE: An illumination-correction method for optical microscopy. *Nat. Methods* **12**, 404–406 (2015).
54. P. S. Gade, A. M. Robertson, C. Y. Chuang, Multiphoton imaging of collagen, elastin, and calcification in intact soft-tissue samples. *Curr. Protoc. Cytom.* **87**, e51 (2019).
55. F. Thöne, B. Schwanhäusser, D. Becker, M. Ballmaier, D. Bumann, FACS-isolation of Salmonella-infected cells with defined bacterial load from mouse spleen. *J. Microbiol. Methods* **71**, 220–224 (2007).
56. M. Sheppard *et al.*, Dynamics of bacterial growth and distribution within the liver during Salmonella infection. *Cell. Microbiol.* **5**, 593–600 (2003).
57. S. Helaine *et al.*, Internalization of Salmonella by macrophages induces formation of nonreplicating persisters. *Science* **343**, 204–208 (2014).
58. S. M. Lewis, A. Williams, S. C. Eisenbarth, Structure and function of the immune system in the spleen. *Sci. Immunol.* **4**, eaau6085 (2019).
59. J. M. den Haan, G. Kraal, Innate immune functions of macrophage subpopulations in the spleen. *J. Innate Immun.* **4**, 437–445 (2012).
60. R. N. Nix, S. E. Altschuler, P. M. Henson, C. S. Detweiler, Hemophagocytic macrophages harbor *Salmonella enterica* during persistent infection. *PLoS Pathog.* **3**, e193 (2007).
61. N. A. Burton *et al.*, Disparate impact of oxidative host defenses determines the fate of *Salmonella* during systemic infection in mice. *Cell Host Microbe* **15**, 72–83 (2014).
62. P. Moine *et al.*, In vivo efficacy of a broad-spectrum cephalosporin, ceftriaxone, against penicillin-susceptible and -resistant strains of Streptococcus pneumoniae in a mouse pneumonia model. *Antimicrob. Agents Chemother.* **38**, 1953–1958 (1994).
63. J. B. Meinen, J. T. McClure, E. Rosin, Pharmacokinetics of enrofloxacin in clinically normal dogs and mice and drug pharmacodynamics in neutropenic mice with *Escherichia coli* and staphylococcal infections. *Am. J. Vet. Res.* **56**, 1219–1224 (1995).
64. T. Trouchon, S. Lefebvre, A review of enrofloxacin for veterinary use. *Open J. Vet. Med.* **6**, 40–58 (2016).
65. F. Pirro, M. Edingloh, N. Schmeer, Bactericidal and inhibitory activity of enrofloxacin and other fluoroquinolones in small animal pathogens. *Compendium Cont. Edn Pract. Vet.* **21**, 19–25 (1999).
66. P. Kanvatirth *et al.*, Dual role of splenic mononuclear and polymorphonuclear cells in the outcome of ciprofloxacin treatment of *Salmonella enterica* infections. *J. Antimicrob. Chemother.* **75**, 2914–2918 (2020).
67. B. Prideaux *et al.*, The association between sterilizing activity and drug distribution into tuberculosis lesions. *Nat. Med.* **21**, 1223–1227 (2015).
68. M. A. Nolte *et al.*, A conduit system distributes chemokines and small blood-borne molecules through the splenic white pulp. *J. Exp. Med.* **198**, 505–512 (2003).
69. E. E. Schmidt, I. C. MacDonald, A. C. Groom, Comparative aspects of splenic microcirculatory pathways in mammals: The region bordering the white pulp. *Scanning Microsc.* **7**, 613–628 (1993).
70. N. Beristain-Covarrubias *et al.*, *Salmonella*-induced thrombi in mice develop asynchronously in the spleen and liver and are not effective bacterial traps. *Blood* **133**, 600–604 (2019).
71. G. L. Drusano, D. E. Johnson, M. Rosen, H. C. Standiford, Pharmacodynamics of a fluoroquinolone antimicrobial agent in a neutropenic rat model of Pseudomonas sepsis. *Antimicrob. Agents Chemother.* **37**, 483–490 (1993).
72. S. L. Preston *et al.*, Pharmacodynamics of levofloxacin: A new paradigm for early clinical trials. *JAMA* **279**, 125–129 (1998).
73. J. M. Diver, R. Wise, Morphological and biochemical changes in *Escherichia coli* after exposure to ciprofloxacin. *J. Antimicrob. Chemother.* **18**, 31–41 (1986).
74. X. Liu *et al.*, Pharmacokinetics and pharmacodynamics of enrofloxacin treatment of *Escherichia coli* in a murine thigh infection modeling. *BMC Vet. Res.* **17**, 212 (2021).
75. S. A. Brown, Fluoroquinolones in animal health. *J. Vet. Pharmacol. Ther.* **19**, 1–14 (1996).
76. S. Barat *et al.*, Immunity to intracellular Salmonella depends on surface-associated antigens. *PLoS Pathog.* **8**, e1002966 (2012).
77. T. Dörr, K. Lewis, M. Vulić, SOS response induces persistence to fluoroquinolones in *Escherichia coli*. *PLoS Genet.* **5**, e1000760 (2009).
78. C. S. Waddington *et al.*, An outpatient, ambulant-design, controlled human infection model using escalating doses of Salmonella Typhi challenge delivered in sodium bicarbonate solution. *Clin. Infect. Dis.* **58**, 1230–1240 (2014).

79. H. C. Dobinson *et al.*, Evaluation of the clinical and microbiological response to Salmonella Paratyphi A infection in the first paratyphoid human challenge model. *Clin. Infect. Dis.* **64**, 1066–1073 (2017).
80. J. A. Crump *et al.*, Emerging Infections Program FoodNet and NARMS Working Groups, Clinical response and outcome of infection with Salmonella enterica serotype Typhi with decreased susceptibility to fluoroquinolones: A United States Foodnet Multicenter Retrospective Cohort Study. *Antimicrob. Agents Chemother.* **52**, 1278–1284 (2008).
81. M. A. Bregante *et al.*, Comparative pharmacokinetics of enrofloxacin in mice, rats, rabbits, sheep, and cows. *Am. J. Vet. Res.* **60**, 1111–1116 (1999).
82. T. Ogino, T. Arai, Pharmacokinetic interactions of flunixin meglumine and enrofloxacin in ICR mice. *Exp. Anim.* **56**, 79–84 (2007).
83. A. Forrest *et al.*, Pharmacodynamics of intravenous ciprofloxacin in seriously ill patients. *Antimicrob. Agents Chemother.* **37**, 1073–1081 (1993).
84. A. Aminimanizani, P. Beringer, R. Jelliffe, Comparative pharmacokinetics and pharmacodynamics of the newer fluoroquinolone antibacterials. *Clin. Pharmacokinet.* **40**, 169–187 (2001).
85. T. Trouchon, Sb. Lefebvre, A review of enrofloxacin for veterinary use. *Open J. Vet. Med.* **6**, 40–58 (2016).
86. M. Vlazaki *et al.*, A data-based mathematical modelling study to quantify the effects of ciprofloxacin and ampicillin on the within-host dynamics of *Salmonella enterica* during treatment and relapse. *J. R. Soc. Interface* **17**, 20200299 (2020).
87. O. Cunrath, D. Bumann, Host resistance factor SLC11A1 restricts *Salmonella* growth through magnesium deprivation. *Science* **366**, 995–999 (2019).
88. J. E. Shea, C. R. Beuzon, C. Gleeson, R. Mundy, D. W. Holden, Influence of the Salmonella typhimurium pathogenicity island 2 type III secretion system on bacterial growth in the mouse. *Infect. Immun.* **67**, 213–219 (1999).
89. D. Bumann, Heterogeneous host-pathogen encounters: Act locally, think globally. *Cell Host Microbe* **17**, 13–19 (2015).
90. Y. Wu, M. Vulić, I. Keren, K. Lewis, Role of oxidative stress in persister tolerance. *Antimicrob. Agents Chemother.* **56**, 4922–4926 (2012).
91. D. J. Dwyer *et al.*, Antibiotics induce redox-related physiological alterations as part of their lethality. *Proc. Natl. Acad. Sci. U.S.A.* **111**, E2100–E2109 (2014).
92. F. C. Soncini, E. G. Véscovi, E. A. Groisman, Transcriptional autoregulation of the Salmonella typhimurium phoPQ operon. *J. Bacteriol.* **177**, 4364–4371 (1995).
93. E. A. Groisman *et al.*, Bacterial Mg2+ homeostasis, transport, and virulence. *Annu. Rev. Genet.* **47**, 625–646 (2013).
94. J. Choi, E. A. Groisman, Acidic pH sensing in the bacterial cytoplasm is required for Salmonella virulence. *Mol. Microbiol.* **101**, 1024–1038 (2016).
95. G. Sakoulas, M. Kumaraswamy, A. Kousha, V. Nizet, Interaction of antibiotics with innate host defense factors against *Salmonella enterica* Serotype Newport. *MSphere* **2**, e00410–e00417 (2017).
96. L. R. Prost, M. E. Daley, M. W. Bader, R. E. Klevit, S. I. Miller, The PhoQ histidine kinases of Salmonella and Pseudomonas spp. are structurally and functionally different: Evidence that pH and antimicrobial peptide sensing contribute to mammalian pathogenesis. *Mol. Microbiol.* **69**, 503–519 (2008).
97. J. W. Conlan, Critical roles of neutrophils in host defense against experimental systemic infections of mice by Listeria monocytogenes, Salmonella typhimurium, and Yersinia enterocolitica. *Infect. Immun.* **65**, 630–635 (1997).
98. A. P. Vassiloyanakopoulos, S. Okamoto, J. Fierer, The crucial role of polymorphonuclear leukocytes in resistance to Salmonella dublin infections in genetically susceptible and resistant mice. *Proc. Natl. Acad. Sci. U.S.A.* **95**, 7676–7681 (1998).
99. R. M. McCormack *et al.*, Perforin-2 is essential for intracellular defense of parenchymal cells and phagocytes against pathogenic bacteria. *eLife* **4**, e06508 (2015).
100. G. Dougan, V. John, S. Palmer, P. Mastroeni, Immunity to salmonellosis. *Immunol. Rev.* **240**, 196–210 (2011).
101. J. J. Gilchrist, C. A. MacLennan, A. V. Hill, Genetic susceptibility to invasive Salmonella disease. *Nat. Rev. Immunol.* **15**, 452–463 (2015).
102. O. Rossi, A. J. Grant, P. Mastroeni, Effect of in vivo neutralization of tumor necrosis alpha on the efficacy of antibiotic treatment in systemic Salmonella enterica infections. *Pathog. Dis.* **75**, ftx002 (2017).
103. G. Banche, V. Allizond, N. Mandras, V. Tullio, A. M. Cuffini, Host immune modulation by antimicrobial drugs: Current knowledge and implications for antimicrobial chemotherapy. *Curr. Opin. Pharmacol.* **18**, 159–166 (2014).
104. L. Matarazzo *et al.*, Therapeutic synergy between antibiotics and pulmonary toll-like receptor 5 stimulation in antibiotic-sensitive or -resistant pneumonia. *Front. Immunol.* **10**, 723 (2019).
105. G. L. Drusano *et al.*, Interaction of drug- and granulocyte-mediated killing of Pseudomonas aeruginosa in a murine pneumonia model. *J. Infect. Dis.* **210**, 1319–1324 (2014).
106. P. Ankomah, B. R. Levin, Exploring the collaboration between antibiotics and the immune response in the treatment of acute, self-limiting infections. *Proc. Natl. Acad. Sci. U.S.A.* **111**, 8331–8338 (2014).
107. B. R. Levin, F. Baquero, P. P. Ankomah, I. C. McCall, Phagocytes, antibiotics, and self-limiting bacterial infections. *Trends Microbiol.* **25**, 878–892 (2017).
108. Y. Willer, B. Müller, D. Bumann, Intestinal inflammation responds to microbial tissue load independent of pathogen/non-pathogen discrimination. *PLoS One* **7**, e35992 (2012).
109. T. Dolowschiak *et al.*, IFN-γ hinders recovery from mucosal inflammation during antibiotic therapy for Salmonella gut infection. *Cell Host Microbe* **20**, 238–249 (2016).
110. K. T. Feehan, D. W. Gilroy, Is resolution the end of inflammation? *Trends Mol. Med.* **25**, 198–214 (2019).
111. F. M. Aarestrup, C. Wiuff, K. Mølbak, E. J. Threlfall, Is it time to change fluoroquinolone breakpoints for Salmonella spp.? *Antimicrob. Agents Chemother.* **47**, 827–829 (2003).
112. P. Aichele *et al.*, Macrophages of the splenic marginal zone are essential for trapping of blood-borne particulate antigen but dispensable for induction of specific T cell responses. *J. Immunol.* **171**, 1148–1155 (2003).
113. M. B. Fischer *et al.*, The presence of MOMA-2+ macrophages in the outer B cell zone and protection of the splenic micro-architecture from LPS-induced destruction depend on secreted IgM. *Eur. J. Immunol.* **37**, 2825–2833 (2007).
114. D. A. C. Stapels *et al.*, *Salmonella* persisters undermine host immune defenses during antibiotic treatment. *Science* **362**, 1156–1160 (2018).
115. D. Bumann, J. Schothorst, Intracellular salmonella metabolism. *Cell. Microbiol.* **19**, e12766 (2017).
116. T. H. M. Pham *et al.*, Salmonella-driven polarization of granuloma macrophages antagonizes TNF-mediated pathogen restriction during persistent infection. *Cell Host Microbe* **27**, 54–67.e5 (2020).
117. M. F. Goldberg *et al.*, Salmonella persist in activated macrophages in T cell-sparse granulomas but are contained by surrounding CXCR3 ligand-positioned Th1 cells. *Immunity* **49**, 1090–1102.e7 (2018).
118. P. Mastroeni, B. Villarreal-Ramos, C. E. Hormaeche, Effect of late administration of anti-TNF alpha antibodies on a Salmonella infection in the mouse model. *Microb. Pathog.* **14**, 473–480 (1993).
119. J. Y. Sagiv *et al.*, Phenotypic diversity and plasticity in circulating neutrophil subpopulations in cancer. *Cell Rep.* **10**, 562–573 (2015).
120. D. Ciardiello, E. Elez, J. Tabernero, J. Seoane, Clinical development of therapies targeting TGFβ: Current knowledge and future perspectives. *Ann. Oncol.* **31**, 1336–1349 (2020).
121. J. Domínguez-Andrés *et al.*, Inflammatory Ly6C^{high} monocytes protect against candidiasis through IL-15-driven NK cell/neutrophil activation. *Immunity* **46**, 1059–1072.e4 (2017).
122. K. M. Knudson, J. W. Hodge, J. Schlom, S. R. Gameiro, Rationale for IL-15 superagonists in cancer immunotherapy. *Expert Opin. Biol. Ther.* **20**, 705–709 (2020).
123. C. S. Easmon, A. Blowers, Ciprofloxacin treatment of systemic salmonella infection in sensitive and resistance mice. *J. Antimicrob. Chemother.* **16**, 615–619 (1985).
124. G. Nath *et al.*, Does Salmonella Typhi primarily reside in the liver of chronic typhoid carriers? *J. Infect. Dev. Ctries.* **4**, 259–261 (2010).
125. Nath G, Pratap CB, Patel SK, Gulati AK, Tripathi SK (2011) Isolation of Salmonella typhi from apparently healthy liver. *Inf. Genetics Evol.* **11**, 2103–2105.
126. R. W. Crawford *et al.*, Gallstones play a significant role in Salmonella spp. gallbladder colonization and carriage. *Proc. Natl. Acad. Sci. U.S.A.* **107**, 4353–4358 (2010).
127. H. R. Ueda *et al.*, Whole-brain profiling of cells and circuits in mammals by tissue clearing and light-sheet microscopy. *Neuron* **106**, 369–387 (2020).
128. S. T. Malherbe *et al.*, Catalysis TB–Biomarker Consortium, Persisting positron emission tomography lesion activity and Mycobacterium tuberculosis mRNA after tuberculosis cure. *Nat. Med.* **22**, 1094–1100 (2016).
129. B. Steeb *et al.*, Parallel exploitation of diverse host nutrients enhances *Salmonella* virulence. *PLoS Pathog.* **9**, e1003301 (2013).
130. S. K. Hoiseth, B. A. Stocker, Aromatic-dependent *Salmonella typhimurium* are non-virulent and effective as live vaccines. *Nature* **291**, 238–239 (1981).
131. C. Kröger *et al.*, The transcriptional landscape and small RNAs of *Salmonella enterica* serovar Typhimurium. *Proc. Natl. Acad. Sci. U.S.A.* **109**, E1277–E1286 (2012).
132. C. Rollenhagen, D. Bumann, *Salmonella enterica* highly expressed genes are disease specific. *Infect. Immun.* **74**, 1649–1660 (2006).
133. C. Rollenhagen, M. Sörensen, K. Rizos, R. Hurvitz, D. Bumann, Antigen selection based on expression levels during infection facilitates vaccine development for an intracellular pathogen. *Proc. Natl. Acad. Sci. U.S.A.* **101**, 8739–8744 (2004).
134. F. R. Cianfanelli, O. Cunrath, D. Bumann, Efficient dual-negative selection for bacterial genome editing. *BMC Microbiol.* **20**, 129 (2020).
135. A. Nanchen, A. Schicker, U. Sauer, Nonlinear dependency of intracellular fluxes on growth rate in miniaturized continuous cultures of *Escherichia coli*. *Appl. Environ. Microbiol.* **72**, 1164–1172 (2006).
136. Y. Han *et al.*, The logic of single-cell projections from visual cortex. *Nature* **556**, 51–56 (2018).
137. J. de Olmos, H. Hardy, L. Heimer, The afferent connections of the main and the accessory olfactory bulb formations in the rat: An experimental HRP-study. *J. Comp. Neurol.* **181**, 213–244 (1978).